

**EFFECT OF COBALT DOPANTS AND CALCINATION DURATION ON  
VANADIUM PHOSPHATE CATALYSTS FOR SELECTIVE OXIDATION  
OF *n*-BUTANE TO MALEIC ANHYDRIDE**

**CHIN KAH CHUN**

**A project report submitted in partial fulfilment of the  
requirements for the award of the degree of  
Bachelor (Hons.) Chemical Engineering**

**Lee Kong Chian Faculty of Engineering and Science  
Universiti Tunku Abdul Rahman**

**May 2016**

## DECLARATION

I hereby declare that this project report is based on my original work except for citations and quotations which have been duly acknowledged. I also declare that it has not been previously and concurrently submitted for any other degree or award at UTAR or other institutions.

Signature : \_\_\_\_\_

Name : CHIN KAH CHUN

ID No. : 11UEB05409

Date : 16.04.2016

**APPROVAL FOR SUBMISSION**

I certify that this project report entitled “**EFFECT OF COBALT DOPANTS AND CALCINATION DURATION ON VANADIUM PHOSPHATE CATALYSTS FOR SELECTIVE OXIDATION OF *n*-BUTANE TO MALEIC ANHYDRIDE**” was prepared by **CHIN KAH CHUN** has met the required standard for submission in partial fulfilment of the requirements for the award of Bachelor of Engineering (Hons.) Chemical Engineering at Universiti Tunku Abdul Rahman.

Approved by,

Signature : \_\_\_\_\_

Supervisor : **DR LEONG LOONG KONG**  
\_\_\_\_\_

Date : \_\_\_\_\_

The copyright of this report belongs to the author under the terms of the copyright Act 1987 as qualified by Intellectual Property Policy of Universiti Tunku Abdul Rahman. Due acknowledgement shall always be made of the use of any material contained in, or derived from, this report.

© 2015, Chin Kah Chun. All right reserved.

Specially dedicated to  
my beloved parent, supervisor and friends, who are willing to offer their support and  
encouragement during the conduction of project.

## **ACKNOWLEDGEMENTS**

I would like to thank everyone who had contributed to the successful completion of this project. I would like to express my gratitude to my research supervisor, Dr. Leong Loong Kong for his invaluable advice, guidance and his enormous patience throughout the development of the research.

In addition, I appreciate the support from my loving parent and fellow group mates for being thoughtful and helpful during the entire project. I would also like to thank Miss Zoey Kang for providing constant support in carrying out the research. Without their guidance and knowledge, this research would have not come to completion.

**EFFECT OF COBALT DOPANTS AND CALCINATION DURATION ON  
VANADIUM PHOSPHATE CATALYSTS FOR SELECTIVE OXIDATION  
OF *n*-BUTANE TO MALEIC ANHYDRIDE**

**ABSTRACT**

Vanadium phosphate catalysts were prepared by calcining  $\text{VOHPO}_4 \cdot 1.5\text{H}_2\text{O}$  for different duration (24 and 48 hours) under pure nitrogen flow, in order to create anaerobic atmosphere. The synthesis of sesquihydrate precursor involved a two-step procedure in which  $\text{VOPO}_4 \cdot 2\text{H}_2\text{O}$  acted as an intermediate before obtaining the precursor. Interestingly, it enhanced the formation of  $\text{V}^{5+}$  phase in the catalysts. Results from XRD analysis had shown the crystalline sizes decreased under prolong calcination duration, which lead to increment in specific surface area. Scanning electron microscopy clearly showed that catalysts exhibited plate-like crystallites with folded edges, which were similar to petals of flowers that sandwiched together in layered structure. For EDX and ICP, both results presented similar trend, in which the P/V atomic ratio decreased as calcination duration increased. Prolong the duration of  $\text{N}_2$  calcination also resulted in an increment in the amount of oxygen desorbed from  $\text{V}^{4+}$  species. Lastly, as shown in redox titration and TPR analysis, the VPOCo-24 exhibited higher selectivity than VPOCo-48, due to the fair level of  $\text{V}^{5+}$  phase in the catalyst.

## TABLE OF CONTENTS

<b>DECLARATION</b>	<b>ii</b>
<b>APPROVAL FOR SUBMISSION</b>	<b>iii</b>
<b>ACKNOWLEDGEMENTS</b>	<b>vi</b>
<b>ABSTRACT</b>	<b>vii</b>
<b>TABLE OF CONTENTS</b>	<b>viii</b>
<b>LIST OF TABLES</b>	<b>xi</b>
<b>LIST OF FIGURES</b>	<b>xii</b>
<b>LIST OF SYMBOLS / ABBREVIATIONS</b>	<b>xiv</b>
<b>LIST OF APPENDICES</b>	<b>xv</b>

### CHAPTER

<b>1</b>	<b>INTRODUCTION</b>	<b>1</b>
	1.1 Catalytic Oxidation Process	1
	1.2 Fundamental Theory of Catalysts	3
	1.3 Essential Properties of Good Catalysts	4
	1.4 Type of Catalysis	5
	1.5 Role of Adsorption in Heterogeneous Catalysis	7
	1.6 Problem Statement	9
	1.7 Objectives	9
<b>2</b>	<b>LITERATURE REVIEW</b>	<b>10</b>
	2.1 Catalytic Selective Oxidation	10
	2.2 Maleic Anhydride	14
	2.3 Application of Maleic Anhydride	15
	2.4 Production of Maleic Anhydride	16

2.4.1	Selective Oxidation of Benzene	17
2.4.2	Selective Oxidation of <i>n</i> -Butane	18
2.5	Vanadyl Pyrophosphate Catalyst (VO) <sub>2</sub> P <sub>2</sub> O <sub>7</sub>	20
2.6	Preparation of Vanadium Phosphorus Oxide Catalyst	22
2.6.1	Organic Route	22
2.6.2	Aqueous Route	23
2.6.3	Dihydrate Route	23
2.6.4	Sesquihydrate Route	24
2.7	Parameters of Vanadium Phosphorus Oxide Catalyst	24
2.7.1	Calcination Condition	24
2.7.2	Support System	27
2.7.3	Dopant System	28
2.7.4	P/V Ratio	30
2.8	Sonochemistry	31
<b>3</b>	<b>METHODOLOGY</b>	<b>34</b>
3.1	Materials and Gases Used	34
3.2	Methodology	35
3.2.1	Preparation of Undoped VPO Catalyst	35
3.2.2	Preparation of Co-doped VPO Catalyst	37
3.2.3	Preparation of Co-doped VPO Catalyst	37
3.3	Characterization Technique and Instrumentations	38
3.3.1	X-Ray Diffractometer (XRD)	38
3.3.2	Scanning Electron Microscopy Coupled with Energy Dispersive X-ray Spectrometer (SEM-EDX)	42
3.3.3	Redox Titration	44
3.3.4	Inductively Coupled Plasma – Optical Emission Spectroscopy (ICP-OES)	46
3.3.5	Temperature Programmed Reduction (TPR)	48
<b>4</b>	<b>RESULTS AND DISCUSSION</b>	<b>50</b>
4.1	X-Ray Diffraction (XRD)	50
4.2	Scanning Electron Microscopy (SEM)	52

4.3	Energy Dispersive X-ray Spectrometer (EDX)	58
4.4	Inductively Coupled Plasma – Optical Emission Spectroscopy (ICP-OES)	59
4.5	Redox Titration	60
4.6	Temperature Programmed Reduction (TPR)	62
<b>5</b>	<b>CONCLUSION AND RECOMMENDATIONS</b>	<b>65</b>
5.1	Conclusion	65
5.2	Recommendations	66
	<b>REFERENCES</b>	<b>67</b>
	<b>APPENDICES</b>	<b>71</b>

**LIST OF TABLES**

<b>TABLE</b>	<b>TITLE</b>	<b>PAGE</b>
1.1	Oxidation Catalysis in Industry ( <i>Source: Taufiq-Yap, 1997</i> )	2
1.2	Types of Porous Catalyst	5
1.3	Comparison between Homogenous and Heterogeneous Catalysis ( <i>Source: Hattori et al., 1997</i> )	7
1.4	Comparison between Physisorption and Chemisorption	8
2.1	Physical Properties of Maleic Anhydride	15
2.2	Mechanism of Selective Oxidation of <i>n</i> -Butane	18
2.3	BET Surface Areas of VPO Catalysts Prepared by Different Method	33
3.1	Chemicals and Gases for the Synthesis of Cobalt Supported Vanadyl Pyrophosphate Catalysts	34
4.1	XRD Data on Cobalt-doped VPO Catalyst	51
4.2	EDX Element Identification and Atomic P/V Ratio	58
4.3	ICP-OES Element Identification and Atomic P/V Ratio	59
4.4	Average Oxidation State of Vanadium	61
4.5	Total number of oxygen atoms removed from catalyst by reduction in H <sub>2</sub> /N <sub>2</sub>	63

## LIST OF FIGURES

FIGURE	TITLE	PAGE
1.1	Potential Energy Diagram between Catalysed and Non-catalysed Reaction ( <i>Source: Chorkendorff &amp; Niemantsverdriet, 2007</i> )	4
2.1	World Organic Chemical Production in Year 1991 ( <i>Source: American Chemical Society</i> )	10
2.2	Schematic Representation of Location and Reactivity of Nucleophilic and Electrophilic Oxygen ( <i>Source: Labinger, 1990</i> )	12
2.3	Dependence of Selectivity on Oxygen Coverage in the Oxidation of Ethylene with Silver Catalysts ( <i>Source: Callahan &amp; Grasselli, 1963</i> )	13
2.4	Molecular Structure of Maleic Anhydride	14
2.5	Selective Oxidation of Benzene ( <i>Source: Maleic Anhydride, 2009</i> )	17
2.6	Selective Oxidation of <i>n</i> -Butane	20
2.7	Molecular Structure of VPO ( <i>Source: Maleic Anhydride, 2009</i> )	21
2.8	VPA, VPO and VPD routes for Preparation of VOHPO <sub>4</sub> ·0.5H <sub>2</sub> O precursor ( <i>Source: Hutchings, 2004</i> )	22
2.9	Evolution of VPO Catalyst Performance Correspond to Change in Calcination Duration ( <i>Source: Abon et al., 1997</i> ).	25
2.10	Structure of Doped Catalyst	28
2.11	Influence of Amount of Oxygen Atoms Removed from the Reduction Peak Associated with V <sup>4+</sup> on the <i>n</i> -butane Conversion	30
2.12	Cavitation Process	32

2.13	Comparison of XRD Spectra of VPO Catalysts Prepared by Conventional Reflux (CV) and Sonochemical (US) Method	33
3.1	Preparation of VPO Catalyst	36
3.2	Transition of Color during Reflux for Co-doped VPO	37
3.3	Calcination of Co-doped VPO Catalyst ( $\text{VOHPO}_4 \cdot 0.5\text{H}_2\text{O}$ )	38
3.4	Working Principle of X-Ray Diffractor	39
3.5	Braggs' Law, in which the Incident X-rays Scattered by Atoms in an Orderly Arranged Lattice Planes.	40
3.6	Shimadzu Diffractometer Model XRD-6000	41
3.7	Schematic Diagram of SEM	43
3.8	Hitachi S3400N	44
3.9	Redox Titration Method Setup	45
3.10	Operating Mechanism of ICP-OES	47
3.11	Perkin Elmer Optical Emission Spectrometer Optima 7000 DV	47
3.12	TPDRO Equipment	48
4.1	XRD Patterns of Precursor and Co-doped VPO Calcined at 24 and 48 hours	50
4.2	SEM micrographs of VPO Catalyst in 0.75% <i>n</i> -butane/air for: (a) 24 hours; (b) 48 hours	54
4.3	SEM micrographs of VPO Catalyst in 1% $\text{O}_2/\text{N}_2$ for: (a) 8 hours; (b) 16 hours; (c) 30 hours	55
4.4	SEM micrographs of Cobalt-doped VPO Catalyst in Nitrogen at (a) 3.0k and (b) 10.0k Magnification for 24 hours	57
4.5	SEM micrographs of Cobalt-doped VPO Catalyst in Nitrogen at (a) 3.0k and (b) 10.0k Magnification for 48 hours	58
4.6	TPR in $\text{H}_2/\text{N}_2$ profiles for VPOs catalysts	62
4.7	Data Chart of TPR in $\text{H}_2/\text{N}_2$ for bulk VPO Catalyst	63

**LIST OF SYMBOLS / ABBREVIATIONS**

$T$	Crystallite Size
$\lambda$	Wavelength
MA	Maleic Anhydride
$\text{VOHPO}_4 \cdot 0.5\text{H}_2\text{O}$	Vanadyl Hydrogen Phosphate Hemihydrate
$\text{VOHPO}_4 \cdot 1.5\text{H}_2\text{O}$	Vanadyl Hydrogen Phosphate Sesquihydrate
$\text{VOPO}_4 \cdot 2\text{H}_2\text{O}$	Vanadyl Phosphate Dihydrate
VPO	Vanadyl Pyrophosphate, $(\text{VO})_2\text{P}_2\text{O}_7$
TPR	Temperature Programmed Reduction
SEM	Scanning Electron Microscopy
EDX	Energy-Dispersive X-ray Spectroscopy
FWHM	Full-Width at Half-Maximum
P/V	Phosphorus to vanadium ratio
VPOCo	Cobalt doped VPO catalyst

**LIST OF APPENDICES**

<b>APPENDIX</b>	<b>TITLE</b>	<b>PAGE</b>
A	Dopant Calculation	71
B	Preparation of Solutions Used in ICP-OES	73
C	Procedure for ICP-OES analysis	78
D	Preparation of Solutions Used in Redox Titration	81
E	Procedure for Redox Titration	84
F	Crystallite Size Measurements by Using Powder XRD Technique	87
G	Calculation of P/V and Co/V mole ratio by using ICP-OES analysis	89
H	Calculation for Average Oxidation State of Vanadium ( $V_{AV}$ )	90
I	Calculation for TPR in $H_2$ Analysis	94
J	Calculation for Reduction Activation Energy ( $E_r$ ) for TPR in $H_2$ Analysis	95

## CHAPTER 1

### INTRODUCTION

#### 1.1 Catalytic Oxidation Process

The development in the science of catalysis and modern society is significantly contributed by the introduction of oxidation reaction (Taufiq-Yap, 1997). Defining in terms of chemistry, oxidation process are the conversions of compounds by means of various oxidizing agent. More than 60% of the chemicals and intermediates catalytically synthesized products from chemistry industry involve oxidation process. Nowadays, catalytic oxidation becomes the fundamental principle in synthesizing large scale of monomers or modifiers, which is widely utilized in the production of synthetic fibers, plastic and chemicals such as ethylene oxides, acrylonitrile, vinyl chloride, maleic and phthalic anhydride (Centi et al., 2000).

The introduction of catalysts has significantly boosted up the performance of oxidation reaction. Catalysis are the driving forces of chemical transformation and play crucial role in the production of transportation fuel, bulk and fine chemicals, as well as curbing the formation of pollutants. A catalyst provides alternative pathway, energetically favourable mechanism to non-catalytic reaction, thus allowing the synthesis to be carried out feasibly under optimum operating pressure and temperature (Chorkendorff & Niemantsverdriet, 2007).

The scientists developed a clear distinction between complete and selective oxidation, in terms of the products synthesised. For complete oxidation, the process contributes the formation of carbon dioxide ( $\text{CO}_2$ ) and water ( $\text{H}_2\text{O}$ ), which is

undesirable under chemical synthesis. Generally, it is practiced to eliminate the presence of organic pollutants in gaseous stream, converting into environmental friendly molecules. However, selective oxidation may synthesize a variety of desired products with remarkable properties and wide applications, in which the rate of production of the desired product overshoot others (Taufiq-Yap, 1997).

In the production of chemicals, oxygen may be embodied into the final products, as in the selective oxidation of *n*-butane to maleic anhydride (MA): or the reaction may be an oxidative dehydrogenation in which oxygen only participates in the reaction without incorporating in the desired product, such as in the conversion of butene to butadiene. As illustrated in Table 1.1, the given examples discuss the role of oxidation catalysis in different branches of industry, showing a wide variety of manufactured products.

**Table 1.1: Oxidation Catalysis in Industry** (Source: Taufiq-Yap, 1997)

Catalytic Oxidation in Different Industry		Catalyst
<b>1</b>	<b>Inorganic Industry</b>	
	Oxidation of ammonia to nitric acid	Pt, Rh
	Oxidation of sulphur dioxide to sulphuric acid	V <sub>2</sub> O <sub>5</sub>
<b>2</b>	<b>Synthetic Rubber</b>	
	Oxydehydrogenation of C <sub>4</sub> to butadiene	(Co, Ni) <sub>3</sub> (PO <sub>4</sub> ) <sub>2</sub>
	Oxydehydrogenation of ethylbenzene to styrene	Fe <sub>2</sub> O <sub>3</sub>
<b>3</b>	<b>Synthetic Fibers</b>	
	Ethylene oxide	Ag/Al <sub>2</sub> O <sub>3</sub>
	Ammoxidation of propene to acrylonitrile	Bi <sub>2</sub> (MoO <sub>4</sub> ) <sub>3</sub>
	Selective oxidation of <i>n</i> -butane to MA	(VO) <sub>2</sub> P <sub>2</sub> O <sub>7</sub>
<b>4</b>	<b>Abatement of Pollution and Environmental Protection</b>	
	Catalytic convertor	Pt/Al <sub>2</sub> O <sub>3</sub>
	Combustion of hydrocarbons in flue gases	CuCo <sub>2</sub> O <sub>4</sub>

## 1.2 Fundamental Theory of Catalysts

Catalysts have been used by human kind for over 2000 years (Fogler, 2006). Catalysts are the substances utilized in order to alter the reaction rate, either by accelerating or decelerating. It does so forming bond with the reactants, allowing the conversion of chemicals to desired products, which detaches easily from the active sites, leaving the latter for next catalytic cycle. In brief, there are certain key aspects to be focused under catalytic processes.

Firstly, the desired products must be synthesised at reasonable rate by means of catalyst, under optimum operating temperature and pressure (Taufiq-Yap, 1997). Generally, the synthesis of products can be controlled by the changes in temperature, pressure, concentration and contact time. Increasing the operating temperature and pressure may significantly boost up the production rate, however the reactors to be operated under such condition becomes more progressive and expensive (Chorkendorff & Niemantsverdriet, 2007). In terms of safety aspect, it may contribute to massive damages and casualties if no proper operation is carried out.

In addition, there are thermodynamics limitation to the conditions in which products can be formed, for example the production of ammonia from nitrogen and hydrogen is impractical to be carried out at 600°C. In contrast, high temperature is necessary to disintegrate the strong triple bonding between nitrogen atoms. Without promoting with iron catalyst, it is difficult to carry out the reaction at desired conversion, even is practical, the operating cost may not be economical. If good yields can be offered at low temperatures and pressures, then it is reasonable to find a catalyst that will operate under the mildest possible conditions, since the use of extreme conditions is very expensive.

Second, it is concurrently important that catalyst provides an alternative and energetically feasible pathway, allowing the reaction to be carried at higher rate with minimal waste and pollutants. For example, the formation of ethylene epoxide always associated with salt as by-product, which traditionally disposed into the river under old and non-catalytic synthesis. By introducing chlorine promoted silver as catalyst, ethylene epoxide can be synthesised directly from the ethylene and oxygen at a selectivity of 90%

without creating waste problem (Chorkendorff & Niemantsverdriet, 2007). At the same time, the catalysts also act as reaction promoter that lower the activation energy, allowing the reaction to be carried efficiently at high rate. The Figure 1.1 gives a clear image on the difference in activation energy between catalytic and non-catalysed reaction.

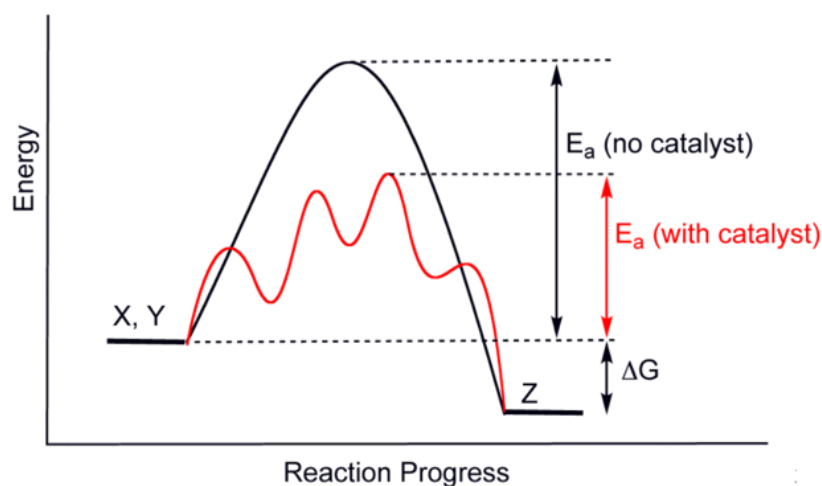


**Figure 1.1: Potential Energy Diagram between Catalysed and Non-catalysed Reaction** (Source: Chorkendorff & Niemantsverdriet, 2007)

### 1.3 Essential Properties of Good Catalysts

Catalysts are generally used to accelerate the rate of chemical reaction, by providing an alternative pathway with lower activation energy for breaking and making of bonds. Much fundamental and applied research is done in order to study the working principle of catalyst and to improve their effectiveness. According to Chorkendorff & Niemantsverdriet (2007), the important physical properties that should be concerned include the particle size and shape, surface area, pore volume, pore size distribution, and strength to resist crushing and abrasion.

In order to achieve significantly optimum reaction rate, the inner porous structure that build up the interfacial area should be studied. Generally, catalyst with fine inner porous structure may contribute to large interfacial area, which is necessary

for high rate of reaction (Fogler, 2006). Catalysts which are classified according to the pores' diameter are as shown in Table 1.2.

**Table 1.2: Types of Porous Catalyst**  
(Source: Bartholomew and Farrauto, 2005)

Type of Structure	Microporous	Mesoporous	Macroporous
Pore Size	Less than 2 nm	In the range of 2 to 50 nm	More than 50 nm

Good catalysts should act as molecular sieves, which contribute the selectivity for the reaction. Since catalysts may exhibit in different pore size, they configure the reactants in such a way that only a certain orientation can react, as well as eliminate the disturbance by larger molecules. An example of such catalyst is zeolite catalysing the formation of para-xylene from toluene and methane (Fogler, 2006).

Besides, resistance to mechanical shear and other extreme conditions is important to determine the effectiveness of the catalyst. It is crucial in which the catalysts are able to be constructed into required shapes without causing undesired pressure drop and hot spots in a reactor. A typical example for such a characteristic is the platinum gauze reactor used in ammonia oxidation of nitric acid, in which platinum acts as the primary material for the monolith (Fogler, 2006).

Lastly, good catalysts are able to maintain their activities at the same catalytic levels for longer periods. In order to increase the shelf life of the catalyst, the catalyst must be regenerated. Regeneration recovers the catalyst to its full potential and prevents the operator from repeatedly purchasing new catalyst.

#### 1.4 Type of Catalysis

Catalyst can present in different of forms, ranging from simple atoms and molecules to large aggregates such as zeolites or alumina. They adapt in different environment

such as gaseous, liquids and solids' surfaces in order to carry out catalytic reaction. Studying the precise composition and shape are the fundamental principles that should be focused in order to prepare catalyst in optimum form. Catalyst can be distinguished into three major types as heterogeneous and homogenous catalysts, as well as biocatalysts. For all catalytic processes, heterogeneous catalysts comprise 80% of the synthesis process, followed by homogenous catalyst and biocatalyst, with coverage 15% and 5% respectively (Concordia, 1990).

In homogenous catalysis, both reactants and catalyst present in the same physical phase, either all molecules are in gas or liquid phase. One of the common examples for homogenous catalysis is atmospheric chemistry. Ozone in the atmosphere can decompose rapidly under the influence of sunlight, however chlorine atoms may speed up the decomposition and leaving in original active state. Since the ozone and chlorine atoms present in gaseous phase, chlorine atoms act as homogenous catalyst for ozone decomposition (Chorkendorff & Niemantsverdriet, 2007). Moreover, metal salts of organic acids, organometallic complexes and carbonyls of Co, Fe, and Rh element are typical homogeneous catalysts. Examples of homogeneously catalysed reaction are carbonylation of methanol to acetic acid with the aid of  $[\text{Rh}(\text{CO})_2\text{I}_2]^-$  complexes in solution.

Heterogeneous catalysis are generally explained as reactions involve different phase of reactants and catalyst. For solid catalysts, unless they are present with high porosity, in which the catalytic reaction may occur on surface active sites. One of the examples of heterogeneously catalyzed reactions is catalytic convertor that clean the automobile exhaust into less hazardous components on noble metal surface such as platinum. The conversion initiates with the adsorption of carbon monoxide and oxygen gas molecules on the surface of catalyst. The platinum catalyst lowers down the activation energy by dissociating the strong bonded oxygen gas into two atoms, encouraging the conversion to carbon dioxide. The carbon dioxide molecules are stable and unreactive, detaches from the active site, liberating the latter for next catalytic cycle. In addition, the rate of dehydrogenation of cyclohexane to produce benzene can be significantly boosted up by using platinum-on-alumina.

**Table 1.3: Comparison between Homogenous and Heterogeneous Catalysis***(Source: Hattori et al., 1997)*

	Homogenous Catalysis	Heterogeneous Catalysis
1	Both the reactants and catalyst are in the same phase.	The reactants and catalyst are in different phase. Generally solid catalysts are utilized to speed up the reactions involves gas or liquid molecule.
2	High dispersion enhancing the activity and selectivity	Low dispersion upsetting the activity and selectivity
3	High diffusivity	May encounter diffusivity problem, results in mass-transfer-controlled reaction
4	High heat transfer	Low heat transfer. May be issue for catalyst with significant difference in heat capacities with reactants
5	High cost of separation : Chemical decomposition and distillation	Low cost of separation : Filtration

### 1.5 Role of Adsorption in Heterogeneous Catalysis

MA is synthesised via selective oxidation of *n*-butane with the aid of VPO catalyst. The reaction is defined as heterogeneous catalysis, since both reactants and catalyst are present in different phase. Under heterogeneous catalysis, adsorption of reaction species acts as rate-limiting path, in order to improve the performance of the catalyst, as well as the catalytic reaction mechanism. The catalytic surface may dispersed with unsaturated bonds, in which these bonding result the reactant molecules to get attached to the catalyst surface. The nature of adsorbate and adsorbent are important parameter in defining the degree of interaction.

Depending on the nature of interaction, adsorption is classified into physisorption and chemisorption respectively. Since only chemisorbed species act as intermediate in catalytic reactions, it is important to master the knowledge of adsorption type (White, 1990). Physisorption is caused by the weak interaction characterized by lack of significant chemical bond between adsorbate and adsorbent, which include dipole and dispersive forces and thus, physisorption helps to define the specific surface area for the catalyst and its support. On the contrary, chemisorptions are associated with sharing or transfer of electrons between participating atoms, resulting in the formation of a chemical bond. In short, chemisorptions helps to determine the area of available active sites under a catalyst.

Table 1.4 gives a comparison between physical and chemical adsorption. These two types of adsorption can be distinguished with the aid of electrical conductivity and infrared (IR) spectroscopy to identify the surface sites using probe molecules (Viswanathan et al., 2002).

**Table 1.4: Comparison between Physisorption and Chemisorption**

	Physisorption	Chemisorption
1	Low heat of adsorption, ranging from 20 to 40 kJ mol <sup>-1</sup>	High heat of adsorption, ranging from 40 to 400 kJ mol <sup>-1</sup>
2	Dominant forces are Van der Waal's forces	Dominant force are chemical bonding, via sharing and transferring of electrons
3	Takes places at low temperature in which higher temperature may inhibit the adsorption	Take place at higher temperature
4	Reversible	Irreversible
5	Formation of multi-molecular layers	Formation of mono-molecular layer

## **1.6 Problem Statement**

To date, the optimum selectivity and activity for VPO catalyst in the production of MA are still in extensive studies. Based on the production information from BASF Petronas (2010), the maximum conversion (activity) of VPO catalyst attempted was at 82 % with 65 % selectivity. It is yet to determine the potential of reduction duration in improving the catalytic performance of VPO catalyst to produce MA. As such, this research will study the effect of various reduction duration, which are 24 and 48 hours, applied to enhance the existing VPOCo catalyst in the hope to increase its selectivity.

## **1.7 Objectives**

1. To synthesise Co doped vanadyl pyrophosphate catalyst via sesquihydrate precursor route.
2. To study the effect of calcination duration towards the physical and chemical properties of cobalt-doped VPO catalysts.

## CHAPTER 2

### LITERATURE REVIEW

#### 2.1 Catalytic Selective Oxidation

Under the modern chemical industry, catalytic selective oxidation processes cover a wide range of commercial application, ranging from large scale production of marketable products to minute amount of fine chemicals. The Figure 2.1 discusses the market data for chemicals production in worldwide in 1991. Focusing on the top 50 industrial chemicals, the total production for selective oxidation process accounted for 101.25 billion pounds. In fact, the economic potential of any contribution from this area gave significant values because of its scientific challenge. In worldwide, the selectivity enhancement may contribute about US\$ 1.4 billion from the largest scale of petrochemical oxidation process (Centi et al., 2000).

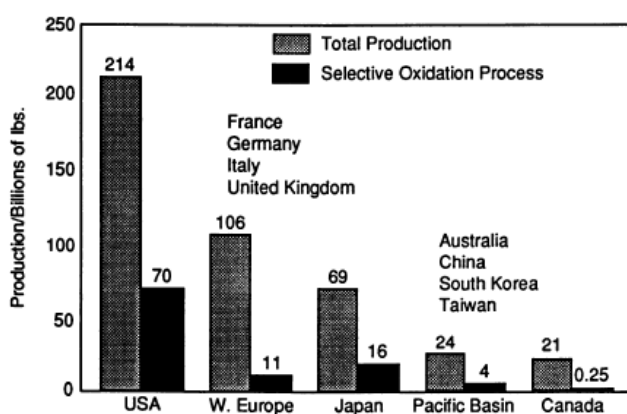


**Figure 2.1: World Organic Chemical Production in Year 1991** (Source: American Chemical Society)

In brief, selectivity is usually considered as the key parameter compared to activity itself under current development of processing industry. The selectivity of a reaction is referring to the fraction of the raw materials convertible to the desired product. The synthesis reaction may involve parallel and sequential reaction, which lower the selectivity of desired products. Selectivity encourages maximum yield of desired products by inhibiting side products, thus lowering costs for purifications. Selectivity for selective oxidation is limited by the tendency for the catalyst to activate the first C-H or C-C bonding of an alkane to form more reactive products and intermediates. In order to achieve desired selectivity, the energy difference should be less than  $40 \text{ kJ mol}^{-1}$ , between reactants and desired products (Hodnett, 1985). Considering the scientific interest, selected issues are discussed in the following statement.

As mentioned above, the initial C-H activation is defined as rate-determining step for selective oxidation, the concentration of lattice oxygen becomes the major concern for optimum process. With presence of hydrocarbon at lattice position of catalyst, the atomic oxygen able to selectively oxidize the component at its core. The reduction of the metal centre is assumed to be occurred due to transportation of  $\text{O}^{2-}$  from core layer of catalyst to its surface. The oxygen in gas-phase are normally treated as undesirable reagents with organics, tend to oxidise the catalyst by obeying the redox chemistry in terms of hydrocarbon and catalyst (Heracleous et al., 2006). This separation is generally defined as Mars-van Krevelan (MvK) reaction, in which the regeneration of catalyst can be carried out at the same temperature for catalytic reaction. Hence, the catalyst maintains its activity towards catalytic reaction, without being re-adsorbed or site-blocked by products.

Second, it is necessary to carry out elemental and structural characterization technique in order to study catalyst in their working state (if possible) because complex composition of mixed oxides, such as VPO favour many oxidation reaction. Similarly, the topography for these complex catalysts need to be analysed under catalytic conditions due to a change in the surface composition. For instance, on Mg-Mn- $\text{O}_x$ , which is widely used oxidative coupling catalyst, the studies concluded that certain proportion of the surface is reduced to a state which different from the original condition (Labinger, 1990). It is crucial to study the structure of catalyst due to

correlation between selectivity and the amount of crystalline faces present. For a high performance oxidation catalyst, it is necessary to be built in multi-phase in order to compensate different requirements in conducting selective oxidation of hydrocarbon at optimum phases in catalytic cycle. The researchers still faced difficulties in quantifying the actual element composition due to the possibility of non-homogeneity problems. However, under recent development in catalyst research have shown that high performance and substantial catalytic cycle can be acquired from single-phase system.

Under accepted principle of oxidation, electrophilic and nucleophilic oxygen types participate in total and selective oxidation respectively. Electron deficient adsorbed species such as superoxide  $O_2^-$ , peroxide  $O_2^{2-}$  and oxide  $O^-$  are typical examples for electrophilic electrons, whereas nucleophilic oxygen covers saturated species with oxygen atom in nominal  $O^{2-}$  state such as terminal oxygen group  $M=O$ , or  $\mu$ -oxo bridging group  $M-O-M$ . Generally, both oxygen types may present in certain ratio in the catalyst structure, which may help to control selective or total oxidation as shown in Figure 2.2. There is qualitative agreement, in which the electrophilic oxygen species may weakly bonded due to the detrimental characteristics of gas phase oxygen. From the observation in which catalytic activity and selectivity remains at the same level without gas phase oxygen supply, it gives credible evidence that kinetic availability of electrophilic oxygen species determine the direction of oxidation, in selective or total pathway. Thus, the kinetic availability for electrophilic oxygen species should be controlled during a catalytic cycle in designing selective oxidation catalysts.

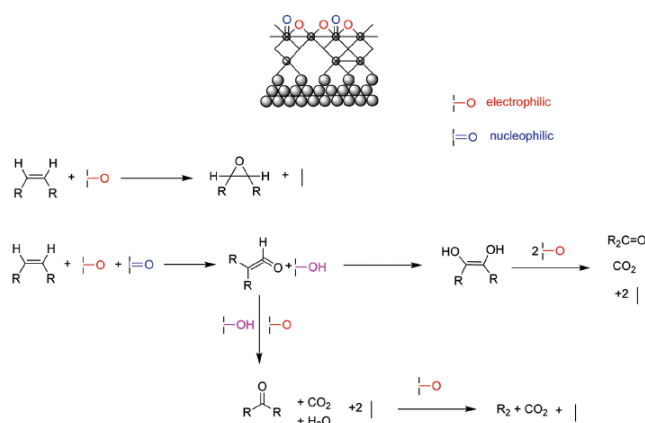


**Figure 2.2: Schematic Representation of Location and Reactivity of Nucleophilic and Electrophilic Oxygen** (Source: Labinger, 1990)

On metal with uniform surfaces, it is obvious that the optimal coverage of adsorbed oxygen for selective oxidation is half of the surface. Although there is no standard theoretical characterization for oxides, the study has proven that the spent oxide catalysts are present in partially reduced state with the aid of ultraviolet-visible spectrometry. As shown in Figure 2.3, the selectivity increases proportionally with oxygen coverage. In order to achieve selective oxidation at maximum selectivity, it is suggested that limiting the number of active oxygen atoms may enhance the reaction of metal oxide partially to 60-70% (Callahan & Grasselli, 1963). Explaining in terms of crystallographic manner, the catalyst structures should exhibit strong variation in atoms density in order to combine locally dense building blocks with polyhedral linkage, leaving substantial vacancy in the unit cell. Salts of heteropolyacids (HPA), with an ideal crystal structure are capable to perform many selective oxidation reactions, presenting a precise example for site isolation. With the presence of isolated sites, the reduced metal minimize the electrons influx, as well as oxygen and hydrogen active species. In short, this may minimize the occurrence for total oxidation. It is necessary to conduct more studies on the surface oxidation state at catalytic condition in order to generate reaction mechanisms as guidance for further catalyst synthesis.

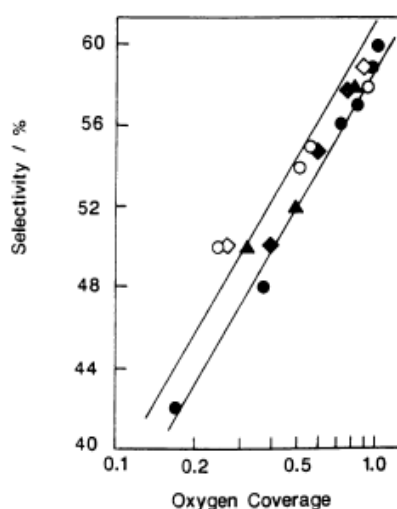


**Figure 2.3: Dependence of Selectivity on Oxygen Coverage in the Oxidation of Ethylene with Silver Catalysts** (Source: Callahan & Grasselli, 1963)

## 2.2 Maleic Anhydride

MA is a colourless organic solid associated with an acrid odour, with the formula  $C_2H_2(CO)_2O$ . With three active sites (two carboxyl groups and one double bond), MA acts as an excellent agent in joining and cross linking, which is widely used in the manufacture of products in market, typically polycondensation of engineering plastics and miscellaneous addition reactions.

Generally, it is widely regarded as one of the most researched organic chemical intermediate for due to its economic potential, as well as its environmentally acceptable properties. Since many organizations have directed their companies' policies to environmental conversation, the utilization of MA may significantly drive the use of more sustainable chemicals to a higher level. As such, much attention has been given to renewable sources or replacing one petroleum-based chemicals with more environmentally friendly products. Based on the recent report by World Petrochemical (WP), global production and consumption of MA were both approximately 1.7 million metric tons in 2010, which is expected to grow an average 19.6 % per year from 2010 to 2020 (World Petrochemical, 2011).

The molecular structure of MA is shown in Figure 2.4, as well as its physical properties in Table 2.1 (Maleic Anhydride, 2009).

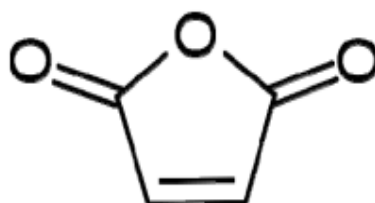


**Figure 2.4: Molecular Structure of Maleic Anhydride**

*(Source: Maleic Anhydride, 2009)*

**Table 2.1: Physical Properties of Maleic Anhydride**

Properties	
Formula	$C_2H_2(CO)_2O$
Molecular Weight	98.06 $gmol^{-1}$
Melting Point	53.58 °C
Boiling Point	200.1 °C
Crystalline Form	Orthorhombic

### 2.3 Application of Maleic Anhydride

MA acts as important feedstock in many chemical processes, notably unsaturated polyester resins (UPR), lube oil additives, copolymers and various agriculture chemicals (Moulijn et al., 1993). Based on market data in 2001, around 63% of MA is used to manufacture UPR (Sundmacher, 2006). The UPR market generally projects the current economic condition since it is strongly bonded to the construction, automobile, marine and fine chemical industries. Normally, UPR are added with chopped glass fibers, which act as reinforcement to produce strong, light-weight, and corrosion resistant material (Felthouse et al., 2001).

It is also widely used as enhancement components in the manufacture of lacquers and lubricant. In lubricant industries, the MA additives reduces the drying period necessary for oil and improves the coating performance of lacquers. Also, the dispersion of MA derivatives prolongs the oil change intervals, thus allowing the automotive engines to perform at high efficiency. The use of MA in the manufacture of agricultural chemicals such as herbicides, pesticides and plant growth regulators is also one of the common applications in market. Pesticides like Malathion and Difolatan are produced by using MA as the major ingredient (Felthouse et al., 2001).

MA can also be used to produce a vinyl copolymer through the copolymerization with vinyl functionality bonded molecules. Typical copolymers are styrene-maleic which is used to produce engineering thermoplastic, paper treatment chemical, floor polishes, adhesives, detergents (acrylic acid-maleic) and cosmetics.

Under biomedical and pharmaceutical field, MA can also copolymerize with mono-O-methyl oligo ethylene to form partially esterified glycol vinyl ethers. The recently developing application for MA is the synthesis of 1,4-butanediol. The synthesis begins with the selective oxidation of *n*-butane to MA, which further reduced to tetrahydrofuran. Almost half of the world production of 1,4-butanediol is dehydrated to tetrahydrofuran to make synthetic fibres like Spandex with exceptional elasticity (Chorkendorff & Niemantsverdriet, 2003).

## 2.4 Production of Maleic Anhydride

In the early 1930s, MA was traditionally produced by selective oxidation of benzene by means of  $V_2O_5$ - $MoO_3$  catalyst. From the molecular formula, we observe that only four carbon atoms are required for the production of MA, hence the presence of extra two carbon atoms in benzene feedstock is considered inefficient (Felthouse et al., 2001).

The earlier synthesis process was replaced with selective oxidation of *n*-butane as a consequence of lower price, widespread availability in the market and no extra carbon lost as CO and  $CO_2$  (Cavani and Trifiro, 2004). In addition, benzene is generally classified as hazardous materials due to its high toxicity and flammability, thus replacement with *n*-butane can eliminate the danger associated in the production. However, the major drawback for the replacement is the best conversion obtained from selective oxidation of *n*-butane is 60%, which is lower than benzene at 71.25% (Lopez et al., 2001). Thus, the performance of *n*-butane selective oxidation was enhanced by the introduction of VPO catalysts, which significantly boosted up the conversion to 80%.

The production of MA using *n*-butane was firstly commercialised at Monsanto's J.F Queeny plant in 1974. In 1978, an estimated value of 341 million pounds of MA was produced (Felthouse et al., 2001). Daxiang Wang and co-workers initiated the selective oxidation of *n*-butane by means VPO catalyst, in order to manufacture MA based on Mars-van Krevelan mechanism. Under the production,

circulating fluidized bed riser reactors were operated at high temperature between 500 – 620 °C, in which reduction and regeneration of VPO catalyst were carried out in spatially separated reactors. However, cyclic experiments shows that there is significant improvement in conversion, selectivity, as well as yield of MA, when the synthesis steps are carried out at temperature range between 416°C and 580°C (Huang et al., 2002).

#### 2.4.1 Selective Oxidation of Benzene

As mentioned in previous section, selective oxidation of benzene in the vapour phase was carried out as the main route in MA production for 50 years. Currently, the synthesis still covers 15 % to 20 % of global capacity outside certain region of United States (Maleic Anhydride, 2009).

The oxidation process can be divided into two steps, the reaction and recovery. The reaction step is a typical process using benzene as a feedstock. A preheated vapour mixture of air and benzene passed through the supported catalyst in fixed bed reactor. The catalyst used kieselguhr alumina or silica supported vanadium oxide. Those supports offer lower surface area because conversion of benzene to MA could be adversely affected by high surface area (Trivedi & Cullbertson, 1982). The principal reaction of the process can be represented by the chemical equation presented in Figure 2.5, in which the ratio of CO to CO<sub>2</sub> is dependant to the reaction state (Maleic Anhydride, 2009).

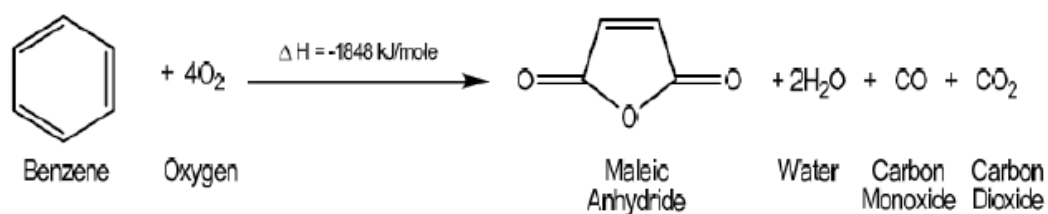


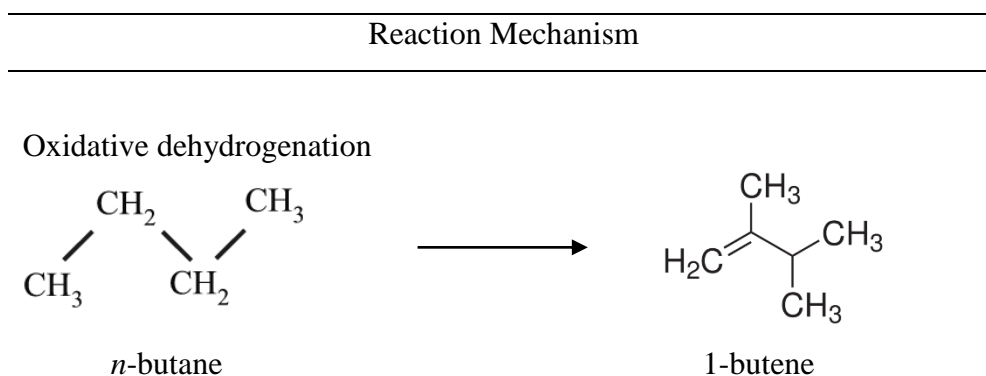
**Figure 2.5: Selective Oxidation of Benzene** (Source: Maleic Anhydride, 2009)

### 2.4.2 Selective Oxidation of *n*-Butane

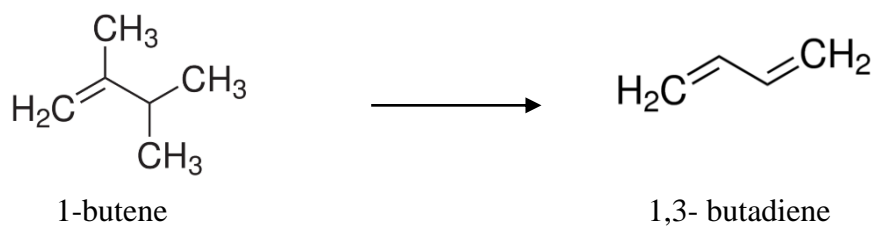
Approximately 225 patents have been discussed on the MA technology in the United States since 1980. This indicates a significant demand from market, thus it is considerable to understand the practicable process enhancement, in order to achieve optimum production. Catalyst, being the driving forces of wide variety of the chemical industry, is earning a lot of focus from the researchers. Previously, three types of catalyst were utilized in the selective oxidation synthesis, namely magnesium orthovanadate,  $Mg_3(VO_4)_2$ , magnesium pyrovanadate,  $Mg_2V_2O_7$  and VPO. As such, extensive studies and researches were carried out, concluded that VPO application significantly boost the conversion of reactant, thus it was chosen to provide catalytic active phase to boost the performance of catalytic synthesis.

Selective oxidation of *n*-butane to MA over the VPO catalysts is recognized as one of the most complicated selective oxidations. The transformation of MA involves participation of following steps, notably elimination of eight hydrogen atoms and addition of three oxygen atoms to a closed ring. It is a redox reaction in which the *n*-butane is partially oxidized by lattice oxygen of catalyst based on Mars-van Krevelan mechanism. The consumed lattice oxygen is then replenished by surface oxygen from gas stream in order to regenerate the catalyst. Due to the detection of butane, butadiene and furan under certain circumstances such as deficiency in oxygen atoms, the researchers proposed a mechanism on the conversion of *n*-butane to MA as shown in Table 2.2, in which the evaluation will be based on further study (Feltouse et al., 2001).

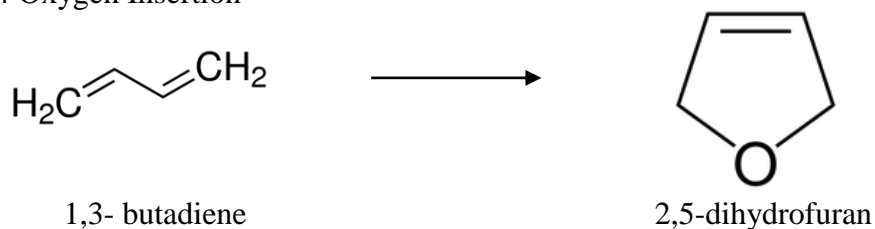
**Table 2.2: Mechanism of Selective Oxidation of *n*-Butane**



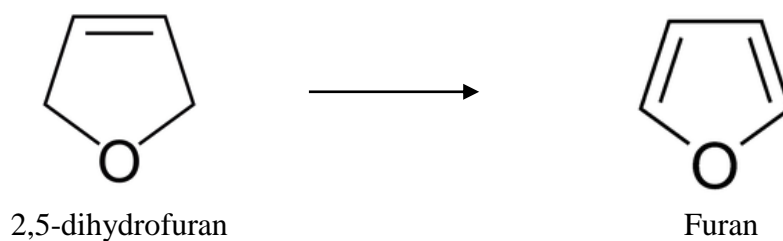
Allylic oxidation



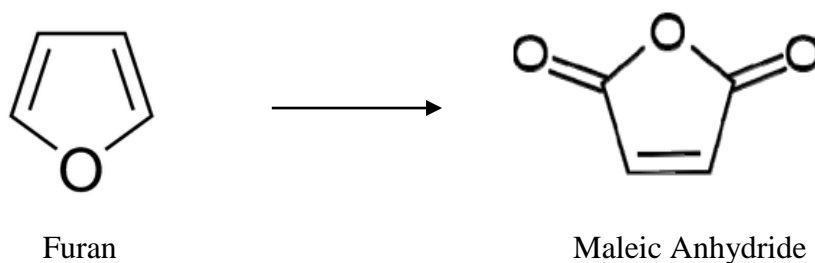
1-4 Oxygen Insertion



Allylic oxidation



Electrophilic oxygen insertion



In the conversion of *n*-butane to MA, the *n*-butane in gas form flow through the VPO catalyst at a temperature of 460°C and a duration around 6 hours. The conversion is highly exothermic, in which the heat of reaction is -1260 kJ/mol and normally associated with total oxidation of hydrocarbon to CO and CO<sub>2</sub>. As the *n*-butane flows through the catalyst, the reactant will absorb on the catalyst's surface in

which the chemical reaction occurs. The lattice oxygen species from the catalyst will be removed by *n*-butane and forms a complex. When this complex desorbs from the catalyst, the final desired product, MA is formed. The chemical reaction is shown in Figure 2.6.

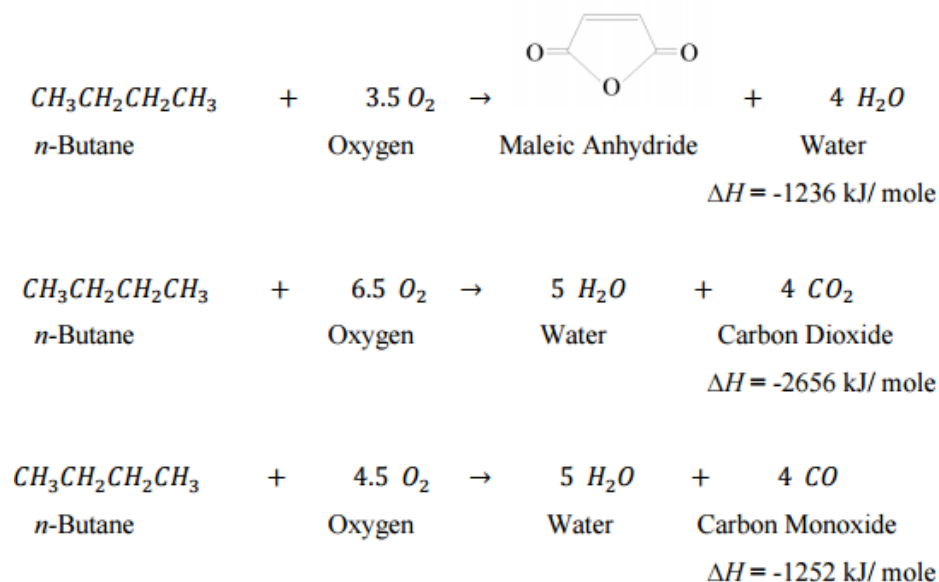


**Figure 2.6: Selective Oxidation of *n*-Butane**

## 2.5 Vanadyl Pyrophosphate Catalyst (VO)<sub>2</sub>P<sub>2</sub>O<sub>7</sub>

Vanadyl pyrophosphate catalyst shows the best configuration of crystallographic phase as selective catalyst for production of MA. It is namely heterogeneous catalytic process, since both reactant and catalyst present in different phase. Besides, VPO catalyst have shown promising catalytic performance in the selective oxidation of propane to acrylic acid, pentane to maleic and phthalic anhydride, as well as the oxidative dehydrogenation of ethane and propane (Datta et al., 2002).

As shown in Figure 2.7, VPO molecules consists of (100) layers, in which each plane is composed of pairs of sharing edge (VO)O<sub>4</sub> square pyramids in trans position, with linkage of phosphate tetrahedral by hydrogen bonding or weak Van der Waals interactions. Each layers are joined by asymmetric V=O-V bond and P-O-P bonds

between structural units (Thompson et al., 2001). In order to enhance the performance of catalyst, intercalation will be carried out in order to improve the accessibility of reactant to the active sites (Datta et al., 2002). As vanadium element presents in oxidation numbers +3, +4 and +5, different VPO phases can be formed with respective morphology and functionality in catalytic system (Abon & Volta, 1997).

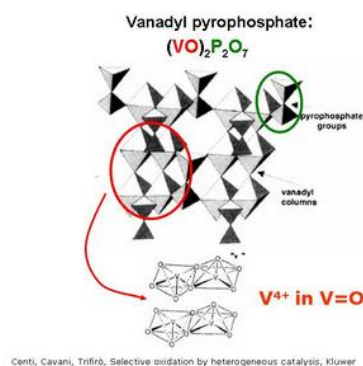


**Figure 2.7: Molecular Structure of VPO** (Source: *Maleic Anhydride*, 2009)

$V^{5+}$  and  $V^{4+}$  are generally the most important phases in VPO catalytic system, in which  $V^{4+}$  phase is responsible for high activity and low selectivity towards MA. Thus, it is obvious that the selectivity to MA is attributed to the presence of limited and controlled amount of  $V^{5+}$  phase at fairly low level (Bartholomew and Farrauto, 2005). This can be explained based on the proposed hypothesis on the surface structure, in which the active site is a mixture of crystalline VPO and an amorphous PVO phase consisting  $V^{5+}$  species. The presence of amorphous PVO phase allows isolation of active centre with clusters of VPO crystalline, thereby limits oxidation of *n*-butane. Hence, the efficiency of partial oxidation of *n*-butane could then be increased (Bartholomew and Farrauto, 2005). However, the desired ratio of  $V^{4+}/V^{5+}$  for best catalytic performance is yet to be justified. The  $V^{5+}$  phase presents in precursor hydrates such as  $VOPO_4 \cdot 2H_2O$ , and precursor hydrates  $VOHPO_4 \cdot 1.5H_2O$  and bulk VPO show the presence of  $V^{4+}$  phase.

## 2.6 Preparation of Vanadium Phosphorus Oxide Catalyst

In 2003, there is a general agreement stated that the best precursor in producing VPO catalyst is  $\text{VOHPO}_4 \cdot 0.5\text{H}_2\text{O}$ , vanadyl hydrogen phosphate hemihydrate precursors (Cornaglia et al., 2003). In recent years, an alternative pathway has been introduced by synthesising VPO catalyst from  $\text{VOHPO}_4 \cdot 1.5\text{H}_2\text{O}$  which contributes to high specific activity in vapour phase oxidation of *n*-butane (Taufiq-Yap et al., 2004). Generally, the preparation is separated into two parts, which are hemihydrate route and sesquihydrate route. Hemihydrate route is further divided into organic route, aqueous route and dihydrate route, as shown in the Figure 2.8.

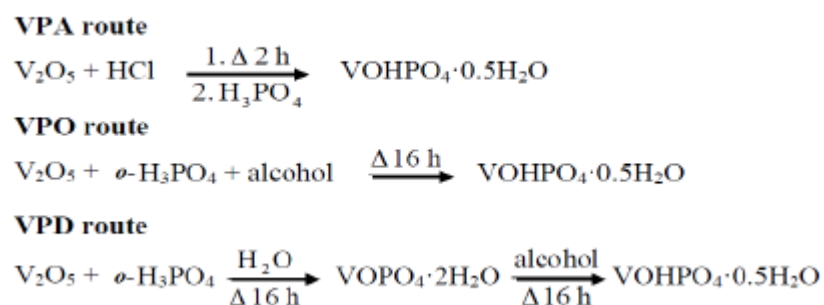


**Figure 2.8: VPA, VPO and VPD routes for Preparation of  $\text{VOHPO}_4 \cdot 0.5\text{H}_2\text{O}$  precursor** (Source: Hutchings, 2004)

### 2.6.1 Organic Route

15 g of  $\text{V}_2\text{O}_5$  was suspended by rapid stirring into 90 mL of isobutanol and 60 mL of benzyl alcohol. The mixture was refluxed for 3 hours at  $120^\circ\text{C}$  under continuous stirring. The colour of the solution changed from brown to black. The mixture was then cooled to room temperature and left stirring at this temperature overnight.

99 % *o*- $\text{H}_3\text{PO}_4$  was added in a quantity such as to obtain the expected P/V atomic ratio. The resulting solution was again heated to  $120^\circ\text{C}$  and maintained under reflux with constant stirring for 2 hours. The slurry (precursor) was then filtered, washed, and dried at  $150^\circ\text{C}$ . This precursor was calcined in air at  $400^\circ\text{C}$  for 6 hour and then for an additional 3 hour in a mixture of 0.75 % *n*-butane and air (Taufiq Yap et al., 2001).

The organic synthesis route results in platelet crystalline morphology. The size of the platelets and the configuration of packing determined by the selection of organic solvent. During agglomeration of platelets, a rosebud-shape morphology can be observed under synthesis with isobutanol. Large alcohols such as, benzyl alcohol, appear to produce platelets with stacking faults which can be deduced from the broadening of the (200) reflection in XRD (Benziger et al., 1997).

### 2.6.2 Aqueous Route

15 g of  $V_2O_5$  was dissolved in 200 mL of 37 % HCl and the mixture was refluxed for 3 hours at  $120^\circ\text{C}$  under continuous stirring to ensure completion reduction to  $V^{4+}$  phase. 85 % *o*- $H_3PO_4$  was added in a quantity such as to obtain the expected P/V atomic ratio. Since the solution is strongly acidic, no precipitation occurs at this stage. The resulting solution was again heated to  $120^\circ\text{C}$  and concentrated to a volume of 20mL. Further evaporation was carried out and precursor was calcined in air at  $400^\circ\text{C}$  for 6 hour and then for an additional 3 hour in a mixture of 0.75 % *n*-butane and air (Taufiq Yap et al., 2001). Comparing the information extracted from XRD analysis, the precursors prepared in aqueous medium are observed to be more crystalline than present in organic medium.

### 2.6.3 Dihydrate Route

15 g of  $V_2O_5$  reacting with 30 mL of 85% of *o*- $H_3PO_4$  in water under reflux for 24 hours. Yellowish solid,  $VOPO_4 \cdot 2H_2O$  was recovered by filtration and washed with water followed by acetone. The  $VOPO_4 \cdot 2H_2O$  reacted with isobutanol and reflux for 20 hours. The solid product was recovered by filtration and dried in air. This vanadyl phosphate hemihydrate precursor then later activated to vanadium phosphorus oxide.

#### 2.6.4 Sesquihydrate Route

The synthesis of sesquihydrate precursor has been divided into a two-step procedure involving  $\text{VOPO}_4 \cdot 2\text{H}_2\text{O}$  as an intermediate before obtaining the precursor.

Firstly, vanadyl phosphate dihydrate,  $\text{VOPO}_4 \cdot 2\text{H}_2\text{O}$  was prepared by reacting 15g  $\text{V}_2\text{O}_5$  with aqueous 90 mL of 85% *o*- $\text{H}_3\text{PO}_4$  in 180 mL of distilled water. The mixture was then stirred under reflux at 393 K for 24 h. The orange-brownish solid solution has gradually changed to yellow. The resultant yellow solid was then recovered by using centrifuge technique and subsequently washed sparingly with distilled water and oven dried at 353K for 16 h.

Secondly, 10.0 g of  $\text{VOPO}_4 \cdot 2\text{H}_2\text{O}$  was added to 150 mL of 1-butanol and refluxed at 353K for 24 h. After cooled to room temperature, the resultant precipitates which is whitish-blue powder ( $\text{VOHPO}_4 \cdot 1.5\text{H}_2\text{O}$ ) was centrifuged out from the solvent, washed sparingly with acetone, and dried overnight in an oven at 353 K. The sesquihydrate precursor obtained was calcined at 673K in a reaction flow of 0.75 % *n*-butane/air mixture (Taufiq Yap et al., 2004).

### 2.7 Parameters of Vanadium Phosphorus Oxide Catalyst

The performance of VPO catalyst in the selective oxidation of *n*-butane to MA, in terms of activity and selectivity could be attributed could be attributed to several essential parameters, notably calcinations of the VPO catalyst precursor, selection of catalyst support material, dopants added to the catalyst and P/V atomic ratio of VPO catalyst. All these parameters are the key factors in determining the performance of VPO catalyst at optimum condition.

#### 2.7.1 Calcination Condition

Calcination is a high-temperature treatment of catalyst precursors in air, which is generally carried in the final step of catalyst synthesis. The main purpose of carrying

out calcination is to transform the precursor to active phase of catalyst, particularly decomposing the presence of impurities during the preparation step (Taufiq-Yap et al., 2007). After the calcination, the bulk VPO catalyst is obtained by eliminating water molecules from the active phase.

Generally, it is suggested that increasing calcination duration on VPO hemihydrate precursor to nitrogen environment at 1073 K decreases the surface area of the catalyst. In addition, it enhances the mobility of oxygen lattice and increases the amount of oxygen being removed (Leong et al., 2012). As shown in Figure 2.5, butane conversion and selectivity for maleic anhydride formation significantly increase with time of calcination, to ensure certain reduction of  $V^{5+}$  to  $V^{4+}$ . The concentration of  $V^{5+}$  should be maintained at fairly low level to ensure good catalytic performance (Abon et al., 1997).

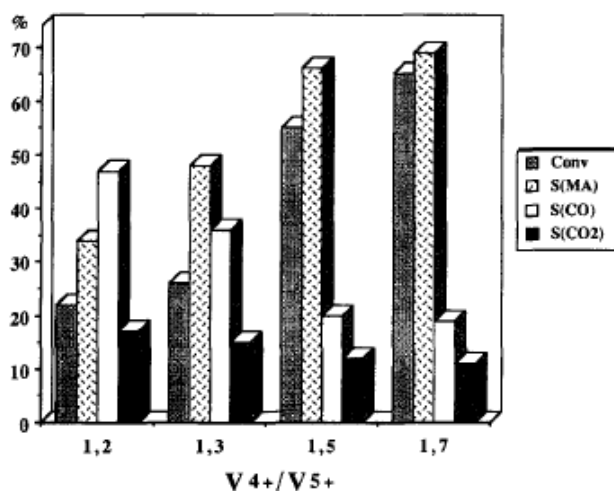


**Figure 2.9: Evolution of VPO Catalyst Performance Correspond to Change in Calcination Duration** (Source: Abon et al., 1997).

However, based on the research under Taufiq Yap et al. (2001), the study concluded that increasing calcination duration on sesquihydrate precursor reduced the surface area, as well as produced rougher and cracked surface of crystal platelet. Thus, the parameter concerned in this technical report is to determine the optimum duration for the calcination to be carried out.

Aside from calcination duration, calcination temperature also serves as important parameter in enhancing the catalytic performance of VPO catalyst. An increasing calcination temperature may enhance the crystallinity by means of agglomeration process to form desired shape of catalyst.

Patience et al. (2007) has proven that activation of the catalysts under continuous flowing of gas mixture of *n*-butane and air must be conducted at optimal temperature ranging from 330 to 460°C, to ensure that the catalyst synthesis perform at the best activity and selectivity. However, the catalyst precursor should be kept in the dehumidifier cabinet to avoid entrainment of water molecules, in order to prevent pressure build-up that may result cracking of particulate supports. In addition, sintering may occur due to rapid heat up during calcination, in which decomposition of salt may lead to formation of hot spots at localized high temperature (Bartholomew and Farrauto, 2005).

Lastly, the calcination agent may create different calcination atmosphere, which is critical in determining the activity of the catalyst. The changes in the physical and chemical properties of the VPO catalysts calcined in two different conditions were observed, notably calcinations under *n*-butane/air and propane/air. From the research, it showed that both calcination atmospheres can produced catalyst, exhibiting good crystalline with characteristic peaks of pyrophosphate phase. In addition, the specific area of the catalysts in *n*-butane/air was higher compared to the propane/air condition. Besides, *n*-butane/air calcined catalyst will show higher conversion compared to the propane/air calcined catalyst because more oxygen associated with V<sup>4+</sup> phase were removed. In conclusion, transformation of precursor to active phase and surface properties of the active VPO can be affected by duration, temperature and atmosphere of calcination, in order to enhance the catalytic performance of the catalyst to form the MA (Taufiq-Yap et al., 2008).

### 2.7.2 Support System

A catalyst support are normally porous metal oxides that are inert or participate in the catalytic reaction, contributing high surface area to which catalyst particles are affixed. Supported VPO express superior characteristics, by increasing the yield and selectivity of the catalyst towards the conversion of *n*-butane to MA. It does so by encouraging catalyst particles to disperse evenly at high surface area, thus offers higher amount of actives per unit mass of support (Guliant, 1999). In addition, the collision between the catalysts particles may crush them into smaller pieces, which result undesired pressure build-up in the bed reactor. Hence, catalyst support provides higher mechanical strength to overcome the extreme condition of bed reactor, thus maintains the catalytic performance at desired level.

Among all, alumina, silica and carbon are the most common with magnesia, titania, zirconia, zinc oxide, silicon carbide and zeolites used for particular applications. They are commonly used in the industrial catalytic processes because of their excellent thermal stability which is suitable for highly exothermic reaction and controllable catalyst structure (Bartholomew and Farrauto, 2005).

However, for the supported VPO catalysts, they usually consist of  $V^{5+}$  phases, mostly in  $\alpha$ -VOPO<sub>4</sub> or  $\gamma$ -VOPO<sub>4</sub> form, may exhibit low MA selectivity as well as low *n*-butane conversion according to Burfield et al. (1978). Hence, the selection of metal oxide support should be focused on elements with good reducing properties, for example titania or zirconia. This is because strong bonding between VPO and reducible support may reduce the  $\alpha$ -VOPO<sub>4</sub> or  $\gamma$ -VOPO<sub>4</sub> crystalline to  $V^{4+}$  phase that remarkably improve the catalytic activity (Au et al., 2004). On the other hand, TiO<sub>2</sub> supported VPO may exhibit high selectivity to MA compared to alumina supported VPO. In summary, an optimized concentration between selectivity and activity of VPO catalyst is determined by the introduction of different catalyst support, which is crucial to obtain the best yield of MA in the production (Baerns and Do, 1998)

### 2.7.3 Dopant System

Dopant, also known as promoter, is active foreign atoms which is usually added to catalysts in small amounts to form solid solution in the lattice (Bartholomew and Farrauto, 2005). By itself, the dopant has no catalytic properties, but improve the surface area and morphology of the catalyst in order to enhance the performance.

Promoters are classified into two types, notably structural and chemical. Structural promoters are generally used to improve the activity of catalyst, as well as improve the mechanical properties and prevent sintering. The doping of structural promoters is carried out via intercalation, which is inclusion of molecules into compound with layered structure. Figure 2.6 shows the structure of doped catalyst, in which the dopant is sandwiched between the VPO plates. Thus, it helps to increase the specific surface area for the catalytic reaction due to the spacing between VPO plates, as well as creates better accessibility of reactant to approach the catalytic phase. For chemical promoters, they are additives that added to catalysts during a reaction to improve the effectiveness of the catalyst by altering the electron distribution at the surface. Typical chemical promoters include alkali earth metals or metal oxides (Bartholomew and Farrauto, 2005). The performance of the catalyst can be significantly boosted by addition of appropriate promoters.

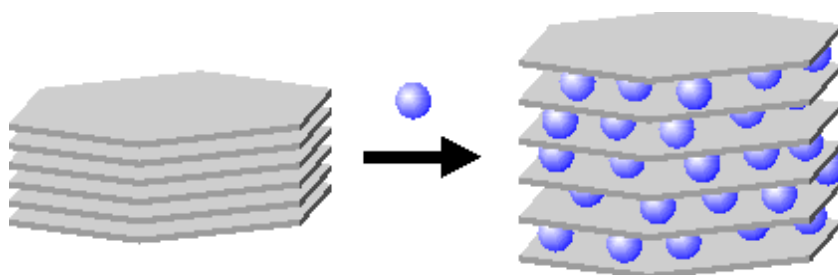


**Figure 2.10: Structure of Doped Catalyst**

Particularly in the selective oxidation of *n*-butane to MA over the VPO catalyst, the dopants help to promote formation of the required VPO compounds and decrease the formation of deleterious phases. Besides, it also enables the formation of solid solutions that regulate the catalytic activity of the solid. A wide range of cations have

been added as the modifiers to catalyst with some beneficial effects. Many studies had shown the influence of the added promoters on the yield and selectivity for maleic anhydride formation as well as the reaction rate over the catalysts. (Bartholomew and Farrauto, 2005)

The scope of study for this research is on cobalt-doped VPO. The VPOCo catalysts is prepared from indirect sonication of  $\text{VOPO}_4 \cdot 2\text{H}_2\text{O}$  with 1-butanol, doped with of cobalt hexahydrate, followed by calcination of  $\text{VOHPO}_4 \cdot 1.5\text{H}_2\text{O}$  at different duration. The addition of cobalt may affect the catalytic performance of VPO formulations. According to Cornaglia et al., they found that redox properties and the acidity of catalysts are significant parameters to be studied in the oxidation of *n*-butane to MA. This is because Lewis sites provide unsaturated  $\text{V}^{4+}$  cations exposed on crystalline plane, which are easily oxidized and hydroxylated. The addition of Co dopant enhances the acidity of VPO and thus increases *n*-butane conversion (Cornaglia et al, 2003).

A good correlation was observed between the oxygen species associated with  $\text{V}^{4+}$  phase and the *n*-butane conversion by plotting conversion versus oxygen species associated with  $\text{V}^{4+}$  as shown in Figure 2.11 for three catalysts (VPO, VPOCr and VPOCo). The result shows that this specific oxygen species was highly active for partial oxidation of *n*-butane in agreement with the electrical conductivity data obtained by Hermann and co-workers. They suggested that the  $\text{O}^-$  species was associated with  $\text{V}^{4+}$  as the centre for the *n*-butane activation. Higher activity of Co-promoted catalysts are due to that these catalysts possess highly reactive and labile oxygen species originated from  $\text{V}^{4+}$  which are capable of increasing the rate for the breaking of C-H bonding, thus increase *n*-butane conversion rate.

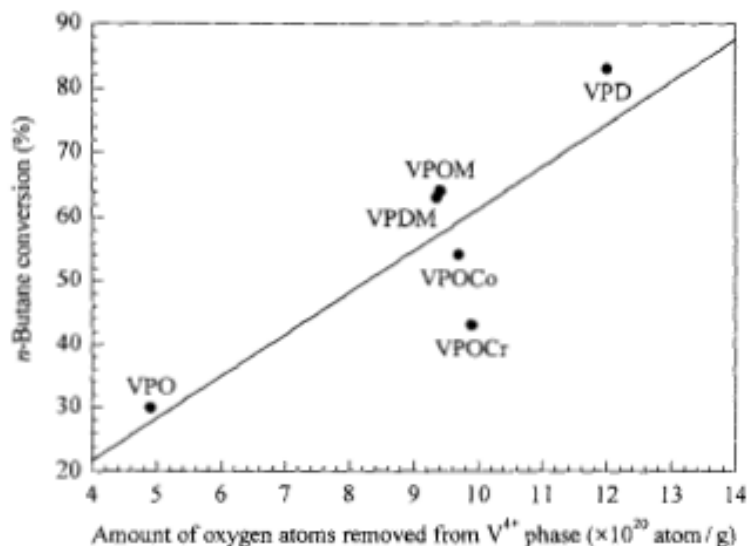


**Figure 2.11: Influence of Amount of Oxygen Atoms Removed from the Reduction Peak Associated with  $V^{4+}$  on the *n*-butane Conversion**

#### 2.7.4 P/V Ratio

The calculation P/V atomic ratio are normally carried out in the early stage of catalyst synthesis, as it strongly determine the final phase composition of catalysts, particularly the distribution of phosphorus and vanadium and its oxidation state (Abon et al., 1997). According to Guliants (2005), an ideal catalyst composition is characterized by a slight excess of phosphate ( $P/V = 1.01-1.10$ ), with respect to empirical formula of  $VOHPO_4 \cdot 1.5H_2O$  precursor. Abon et al. (1997) mentioned that active and selective VPO catalysts present a mean oxidation state of vanadium slightly higher than 4.0 usually associated with P/V ratio of slight higher than 1.0. An excess in phosphorus content may delay the oxidation of  $V^{4+}$  to  $V^{5+}$ , because the former phase may contribute to high conversion of *n*-butane to MA. It does so by terminating side faces plane of bulk catalyst in the form  $VO(PO_3)_2$ , characterized by a lower oxidizability (Matsuura and Yamazaki, 1990). However, further studies showed that the P/V atomic ratio should be controlled at 1.5 to encourage certain oxidation of  $V^{4+}$  to be carried out, since a fairly low level of  $V^{5+}$  phase may enhance the selectivity for MA.

## 2.8 Sonochemistry

Vanadium Phosphorus Oxide (VPO) catalysts are commercially used in the production of maleic anhydride from n-butane. It is generally agreed upon that the best catalyst precursor is  $\text{VOHPO}_4 \cdot 1.5\text{H}_2\text{O}$  which is converted to  $(\text{VO})_2\text{P}_2\text{O}_7$  during activation. This system is generally interest because it is the only heterogeneously catalyzed alkane selective oxidation reaction in commercial use (Centi et al., 1988). However, the low selectivity of this catalyst for maleic anhydride remains a serious problem. Therefore, there is a need to develop new, functional forms of  $(\text{VO})_2\text{P}_2\text{O}_7$  to improve this oxidation process. Since the microstructure, that is the shape and dimensions, of  $(\text{VO})_2\text{P}_2\text{O}_7$  crystallites is generally considered to be a great influence on the catalyst's performance, control over this is a promising approach to improve the catalytic performance of  $(\text{VO})_2\text{P}_2\text{O}_7$  crystallites (Kamiya et al., 2006). Nanotechnology has gained substantial popularity recently due to the rapidly developing techniques both to synthesize and characterize materials and devices at the nano scale, as well as the promises that such technology offers to substantially expand the achievable limits in many different fields including medicine, electronics, chemistry and engineering. Nano size noble metal particles have occupied a central place in heterogeneous catalysis for many years, long before recognition of nanotechnology (Kung & Kung, 2004).

Thus, it is fitting to synthesis nanostructured VPO catalysts via nanostructured  $\text{V}_2\text{O}_5$  obtained through sonochemical treatment. It is found that ultrasound irradiation method allows the synthesis to be carried out in a relatively shorter time of 1 h, with similar surface composition and better hydrocarbon oxidation activity compared with that prepared by reflux method. Ultrasound shows diverse effects on chemical processes, involving organic synthesis, catalytic reactions, and environmental and engineering sciences (Unnikrishnan et al., 2003).

Ultrasonic irradiation enhances the chemical reaction and mass transfer via the process of acoustic cavitation, in which the radiation is transmitted through a medium via pressure waves. Induced-vibrating molecules compress and stretch the molecular structure of the medium due to a time-varying pressure. In the surface vicinity,

ultrasonic streaming produces strong convective currents, which cause a reduction in the thickness of diffusion layers thereby enhancing diffusion-controlled processes.

Molecules start to oscillate at their mean positions and create cavities within liquid if the strength of the acoustic field is sufficiently intense, as well as the presence of surface imperfections or trapped gas can act as the nuclei for bubble formation. The process is known as cavitation as the local tensile strength of the liquid is dominated by negative pressure. There are two types of cavitation, namely stable and transient. Stable cavities are bubbles, which form and oscillate at their equilibrium position over continuous rarefaction/compression cycles, before collapsing or never collapsing at all. A transient cavity exists for only a few acoustic cycles. It means that the bubbles grow during the expansion phase of the sound wave, followed by a shrinking phase and a violent collapse as shown in Figure 2.12. This collapse generates very high pressures and temperatures, hence resulting rapid motion and dispersive effect due to interparticle collisions. The chemical and physical effects of ultrasound are the results of both stable and transient cavities.

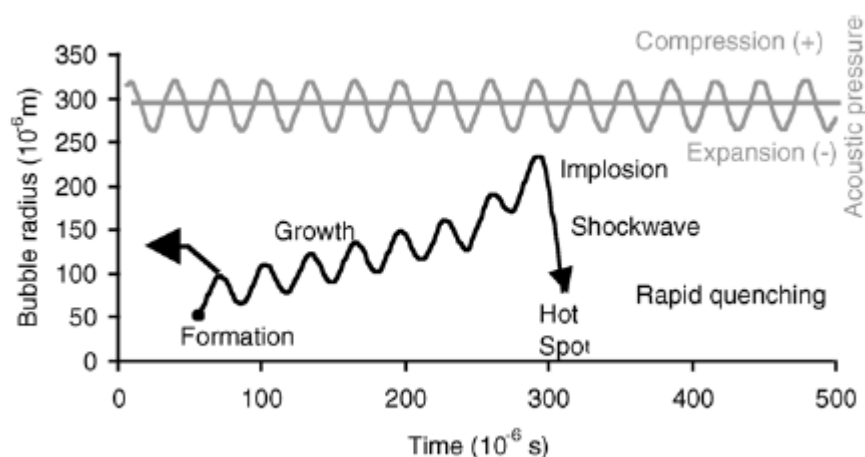


**Figure 2.12: Cavitation Process**

As shown in Figure 2.13, the conventionally prepared VPO catalyst shows peaks at  $2\theta$  values of  $23.1^\circ$ ,  $28.4^\circ$  and  $29.9^\circ$  which characterize the presence of  $(VO)_2P_2O_7$  phase, as well as  $VOPO_4$  phase at  $2\theta$  values of  $22.0^\circ$ ,  $26.0^\circ$  and  $28.9^\circ$ . The XRD spectra of the VPO prepared by 3 h ultrasound irradiation method shows a more amorphous nature containing predominantly vanadyl pyrophosphate (VPP) phase. Increase in the ultrasound irradiation period increases the crystallinity and shows more

sharp peaks of VPP in addition to small amount of VOPO<sub>4</sub> phases. The compositional similarity of the VPO catalyst prepared by the sonochemical method to that prepared by the conventional route suggests that the catalyst preparation can be accomplished much faster using ultrasound irradiation. The strong XRD peak at 29.9° and a relatively weak peak at 26° and 28.9° also suggest that vanadium in the calcined catalyst sample is predominantly in V<sup>4+</sup> state with some amount of V<sup>5+</sup> species. The BET surface area of the calcined VPO catalyst prepared by ultrasound irradiation method (10.3 m<sup>2</sup>g<sup>-1</sup>) is also found to be comparable to that prepared by conventional reflux method (10.2 m<sup>2</sup>g<sup>-1</sup>) as presented in Table 2.3. Figure 2.13 summarizes the XRD spectra of the calcined catalysts prepared by the sonochemical method and its comparison with that prepared by the conventional method (Unnikrishnan et al., 2003)

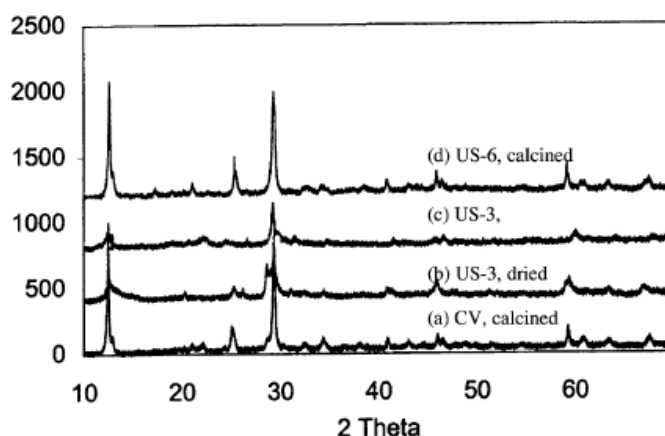


**Figure 2.13: Comparison of XRD Spectra of VPO Catalysts Prepared by Conventional Reflux (CV) and Sonochemical (US) Method**

**Table 2.3: BET Surface Areas of VPO Catalysts Prepared by Different Method**

VPO preparation method	Notation used	BET surface area (m <sup>2</sup> g <sup>-1</sup> cat)
Conventional, reflux (20h)	CV	10.2
Sonication (3 h)	US-3	9.8
Sonication (6 h)	US-6	10.3
Microwave (1 step (1 h))	MW-1S	4.5
Microwave (2 steps (1 h))	MW-2S	12.5
Microwave (2 steps (2 h))	MW-2H	16.8

## CHAPTER 3

### METHODOLOGY

#### 3.1 Materials and Gases Used

The chemicals and gases used throughout the study are listed in Table 3.1.

**Table 3.1: Chemicals and Gases for the Synthesis of Cobalt Supported Vanadyl Pyrophosphate Catalysts**

	Company
Vanadium (V) Pentoxide, $V_2O_5$	MERCK
85% <i>ortho</i> -Phosphorus acid, <i>o</i> - $H_3PO_4$	MERCK
Cobalt (II) Nitrate Hexahydrate $Co(NO_3)_2 \cdot 6H_2O$	
1-Butanol, $CH_3(CH_2)_3OH$	R & M CHEMICAL
Nitric Acid, $HNO_3$	R & M CHEMICAL
Chemicals Sulphuric Acid, $H_2SO_4$	MERCK
Potassium Permanganate, $KMnO_4$	FISHER SCIENTIFIC
Ammonium Iron (II) Sulphate, $(NH_4)_2Fe(SO_4)_2$	R&M CHEMICAL
Diphenylamine, $Ph_2NH$	ACROS
Ammonium Dihydrogen Phosphate, $NH_4 H_2 PO_4$	MERCK
Ammonium Metavandate, $NH_4VO_3$	MERCK

	99.99% Purified Nitrogen	Malaysia Oxygen Berhad, MOX
	99.99 % Purified Helium	Malaysia Oxygen Berhad, MOX
Gases	99.99 % Purified Argon	Malaysia Oxygen Berhad, MOX
	Liquefied Nitrogen Gas	Malaysia Oxygen Berhad, MOX
	Compressed Air	Malaysia Oxygen Berhad, MOX

---

## 3.2 Methodology

In the study, bulk VPO catalyst was developed from the precursor vanadyl hydrogen phosphate sesquihydrate,  $\text{VOHPO}_4 \cdot 1.5\text{H}_2\text{O}$ .

The synthesis of  $\text{VOHPO}_4 \cdot 1.5\text{H}_2\text{O}$  was completed in two stages. The first stage began with the synthesis of vanadyl hydrogen phosphate dihydrate,  $\text{VOHPO}_4 \cdot 2\text{H}_2\text{O}$  as an intermediate product from the reaction between  $\text{V}_2\text{O}_5$  and *ortho*- $\text{H}_3\text{PO}_4$ . In the second stage, 1 mol% of cobalt dopant was added to catalyst sample, followed by the reduction of  $\text{VOHPO}_4 \cdot 2\text{H}_2\text{O}$  with 1-butanol. The precursor  $\text{VOHPO}_4 \cdot 1.5\text{H}_2\text{O}$  was further calcinated at different duration to obtain the bulk catalyst.

### 3.2.1 Preparation of Undoped VPO Catalyst

30 g of vanadium pentoxide,  $\text{V}_2\text{O}_5$  was added with 180 mL *ortho*-phosphoric acid, *ortho*- $\text{H}_3\text{PO}_4$  and 360 mL of  $\text{H}_2\text{O}$ . Direct sonication was carried out, in which the ultrasonic probe was immersed into the mixture, in order to agitate with at 10 kHz for one hour. The colour of product changed from orange to yellow, indicating the formation of  $\text{VOPO}_4 \cdot 2\text{H}_2\text{O}$ . Next, the yellowish solution was cooled down to lower temperature before centrifuging it at 3000 rpm for 8 minutes. After that, the solid phase containing  $\text{VOPO}_4 \cdot 2\text{H}_2\text{O}$  was spread evenly on evaporating dishes and left to dry in an oven at

90°C for at least 24 hours. Lastly, dried sample was collected and pounded into powder form and was therefore ready for the next stage. The apparatus setup for  $\text{VOPO}_4 \cdot 2\text{H}_2\text{O}$  synthesis is shown in Figure 3.1.

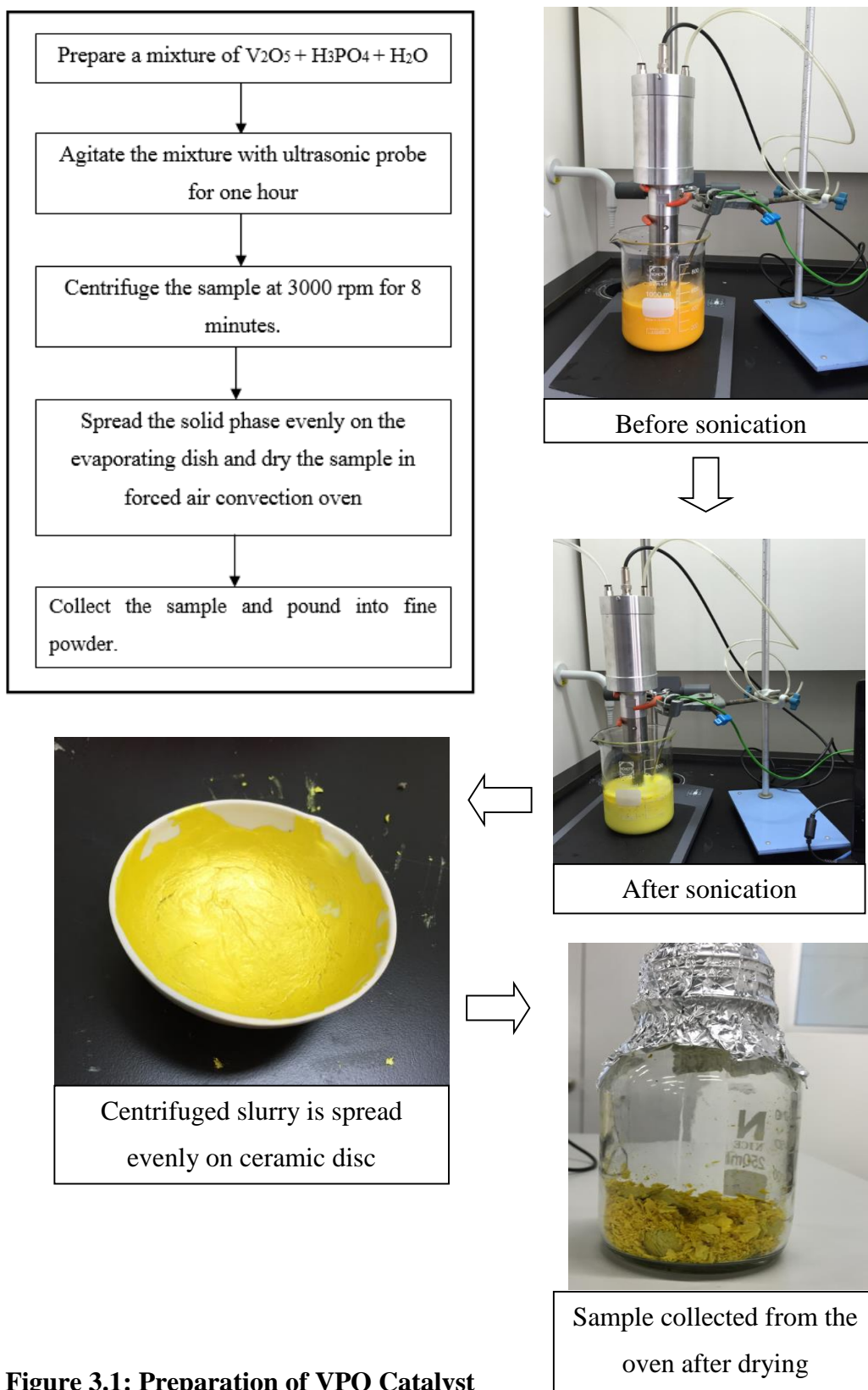


**Figure 3.1: Preparation of VPO Catalyst**

### 3.2.2 Preparation of Co-doped VPO Catalyst

Next, 10 g of  $\text{VOPO}_4 \cdot 2\text{H}_2\text{O}$  bulk intermediate was added with 150 mL 1-butanol and 1 mol % (0.0924 g) of cobalt hexahydrate,  $\text{Co}(\text{NO}_3)_2 \cdot 6\text{H}_2\text{O}$ . The mixture is then refluxed for 24 hours, in which a whitish-blue solution was formed during the reflux process. The transition of mixture is shown in the Figure 3.2. Direct sonication was carried out, in which the ultrasonic probe was immersed into the mixture, in order to agitate with at 10 kHz for one hour. After that, the mixture was cooled down to room temperature before centrifuging it at 3000 rpm for 8 minutes. Next, the solid phase Co-doped vanadyl hydrogen phosphate sesquihydrate,  $\text{VOHPO}_4 \cdot 1.5\text{H}_2\text{O}$  was recovered in an evaporating dish and left to dry in an oven at  $85^\circ\text{C}$  for at least 24 hours. The doped precursor was then pounded into powder form.



**Figure 3.2: Transition of Color during Reflux for Co-doped VPO**

### 3.2.3 Preparation of Co-doped VPO Catalyst

All precursor powders were prepared in several porcelain boats and calcined in a tubular furnace at  $460^\circ\text{C}$ , with a flow mixture of nitrogen at different calcination durations as shown in Figure 3.3.

After calcination, the bulk VPO catalysts were formed and labelled as  $\text{VPOCo-24}$  and  $\text{VPOCo-48}$ , where 24 and 48 are denoted as 24 and 48 hours of calcination duration for cobalt-doped VPO catalyst respectively.

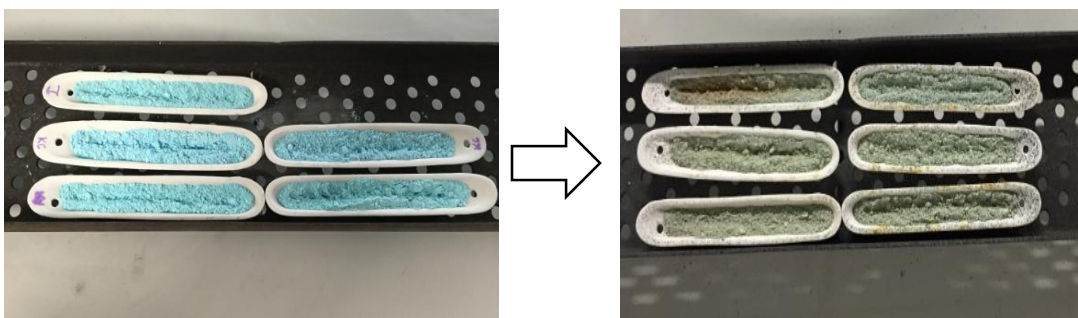


**Figure 3.3: Calcination of Co-doped VPO Catalyst ( $\text{VOHPO}_4 \cdot 0.5\text{H}_2\text{O}$ )**

### 3.3 Characterization Technique and Instrumentations

Throughout the research, different characterization technique and instrumentations were applied to study the physical and chemical properties of the catalyst formed, as well as its reactivity. To determine the physical characteristics, the X-ray Diffractometer (XRD) and Scanning Electron Microscope (SEM) were utilised. As for chemical properties, the catalysts were analysed with EDX (Energy-Dispersive X-ray Spectroscopy), Redox Titration and Inductively Coupled Plasma – Optical Emission Spectroscopy (ICP-OES). The temperature programmed reduction (TPR) was used to determine the reactivity of catalyst, to be more precise, the active sites coverage of the catalyst.

#### 3.3.1 X-Ray Diffractometer (XRD)

In 1912, German physicist Max Von Laue discovered that a crystalline materials can act as three-dimensional diffraction gratings for X-ray, in which the wavelengths are similar to the spacing of planes in a crystal lattice. In the following year, British physicists Sir W.H. Bragg and his son Sir W.L. Bragg developed a relationship to explain the arrangement of atoms in certain crystals, allowing X-ray beams to be reflected at certain angles of incidence. Currently, the XRD is commonly used to perform the following analysis:

- To characterize the crystallographic structure, crystallite size and preferred orientation in polycrystalline or powdered solid samples

- To determine the relative abundance of crystalline elements for heterogeneous solid mixtures, as well as providing structural information on unknown materials
- To study the strains between the crystalline materials
- To monitor the changes in crystalline phases of catalyst by means of lattice structural parameters

X-ray diffraction is based on constructive interference of monochromatic X-rays and a crystalline material. These X-rays are generated by cathode ray tube, by heating the filament to generate high concentration of electrons. These electrons are filtered by using collimator to produce monochromatic radiation, collimated to concentrate and accelerated toward the samples. A notable example is the use of Cu as source to produce  $\text{CuK}\alpha$  radiation. As the bombarding electrons are associated with high energy which is sufficient to dislodge the K-shell electrons, this allows the vacancy to be filled with the electrons from L-shell (Moulijn, 1993). Figure 3.4 shows the working principle of X-ray diffractometer.

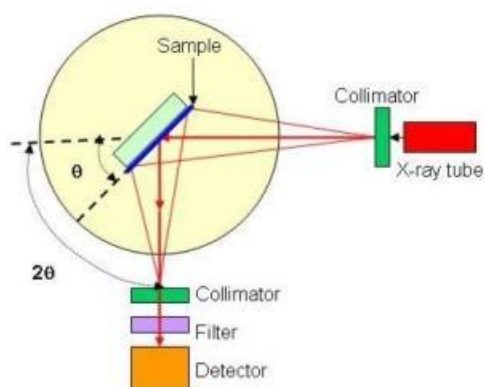


**Figure 3.4: Working Principle of X-Ray Diffractometer**

In general, the term XRD can be explained as the electron scattering of X-rays radiation by atoms of crystalline structure. When conditions satisfying Bragg's Law, the scattered X-rays are separated by interplanar distance  $d$ , producing constructive interference as shown in Figure 3.5. Hence we can measure the lattice spacing,  $d$  by measuring the angle  $2\theta$ , which constructively interfering X-rays with a wavelength,  $\lambda$  leave the crystal applying the Bragg equation (Moulijn, 1993):

$$n\lambda = 2d \sin \theta \quad (3.1)$$

where

$\lambda$  = wavelength

$d$  = lattice plane distance

$\theta$  = diffraction angle

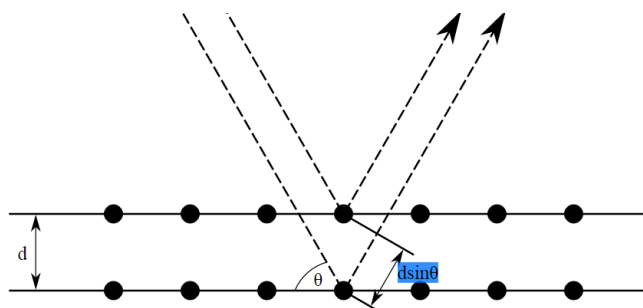


**Figure 3.5: Bragg's Law, in which the Incident X-rays Scattered by Atoms in an Orderly Arranged Lattice Planes.**

Every crystalline material have its own unique lattice arrangement even it is in a mixture, each substance will still give its pattern independently of the others (Hull, 1919). Under our study, XRD analysis is carried out to determine the relative abundance of  $V^{4+}$  and  $V^{5+}$  at ambient temperature. A XRD pattern is obtained by using a movable detector to process and count the characteristic radiation. These patterns may act as “fingerprint” for its identification. The detector scans the intensity of the diffracted radiation as a function of  $2\theta$  between the incoming and the diffracted beams. The detected diffraction pattern of substance is then compared with the standards to identify the unknown material and the areas under the peak are representing the amount of each phase present in the sample. The width of the diffraction peak can be related to the size of the particles being examined by using Debye-Scherrer equation.

$$T = \frac{0.89\lambda}{\beta_{hkl} \cos\theta_{hkl}} \quad (3.2)$$

where

$T$  = crystallite size

$\lambda$  = wavelength

$\beta$  = full-width at half maximum at  $hkl$  phase

$\theta$  = diffraction angle at  $hkl$  phase

The limitation of XRD is due to its characteristic of using interference between reflecting X-rays from the lattice planes. XRD is unable to detect particles with size below  $100 \text{ nm}$  or amorphous, due to occurrence of line-broadening (Chorkendorff & Niemantsverdriet, 2007). This can be crucial if the catalysts contain some particles with very little size, XRD may not detect its presence. Also in rare cases, metal diffraction lines may overlap with the lines from support. The surface region, in which catalytic activity resides are unable to be detected under XRD (Mouljin, 1993).

In this study, XRD pattern were obtained using a Shimadzu diffractometer model XRD-6000, as shown in Figure 3.6, employing  $\text{CuK}\alpha$  radiation generated by a Philips glass diffraction X-ray tube broad focus 2.7 kW type on the catalysts at ambient temperature. The basal spacing was determined via powder technique. The samples were scanned at range  $2\theta = 2^\circ - 60^\circ$  with a scanning rate of  $1.2000^\circ\text{min}^{-1}$ . The diffractograms obtained were matched against the Joint Committee on Powder Diffraction Standards (JCPDS) PDF1 database version 2.6 to confirm the catalysts phase.



**Figure 3.6: Shimadzu Diffractometer Model XRD-6000**

### **3.3.2 Scanning Electron Microscopy Coupled with Energy Dispersive X-ray Spectrometer (SEM-EDX)**

Scanning Electron Microscope (SEM) is a type of electron microscope that is used to provide the imaging of the samples by scanning it with a focused beam of electrons. A stream of electrons is focused onto the sample using magnetic lens, and the interactions between electrons and sample atoms yield backscattered, secondary and X-ray, carrying information such as topography, morphology, composition and crystallographic (Herguth, 2008).

Backscattered electrons are caused by collision of incident electron with an atom in specimen, which results the electron to be backscattered nearly normal to the incident path. The contrast in the image produced is determined by the atomic number of the elements, in which higher atomic number element appears to be brighter. The image will therefore show the distribution of different chemical phases present in the sample (Chorkendorff & Niemantsverdriet, 2007). Because these electrons are emitted from a depth in the sample, the resolution in the image is not as good as for secondary electrons. Secondary electrons are emitted from the atoms occupying the top surface and produce a readily interpretable image of the surface. The contrast in the image is determined by the sample topography and morphology. A high resolution image can be obtained because of the small diameter of the primary electron beam.

Compared to normal light microscope, the electron microscope generates high energy electron source, which can be used to examine the sample on very fine scale, providing detailed and useful information. The magnification of electron microscope can easily reach 250 times higher than the best light microscope can offer under current technology. In addition, the analysed sample under SEM is necessary to be conductive (Radiological and Environmental Management, 2010). If the sample provided is an inorganic, it is necessary to perform sample coating with a thin layer of conductive material such as platinum or gold. Special care should be made to prevent unwanted noise generated during the SEM analysis.

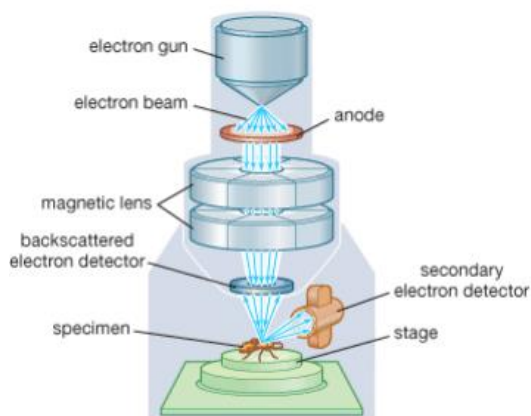


**Figure 3.7: Schematic Diagram of SEM**

*(Source: 2008, Encyclopaedia Britannica, Inc)*

Due to the interaction of the primary beam with atoms in the sample, there is shell transitions which result in the emission of an X-ray. The emitted X-ray associated with the unique characteristic of the elements, which can be detected and measured by Energy Dispersive X-ray Spectroscopy (EDX). The principle of EDX is to detect and collect x-rays being emitted by the particles, converting it to electrical signal and presenting it as a graph of energy versus counts. From there, the EDAX software will compare the result with an element database to identify the peaks.

Under this study, the Hitachi S-3400N is used as analysis machine to characterize the VPOCo catalyst, which is combination of SEM and EDX. A small amount of the samples was placed on the multi sample holder and labelled accordingly. The sample holder was then placed in the sputter coater and coated with a layer of platinum. After the coating process, the sample holder was placed into the SEM and the analysis environment was vacuumed. The test condition is 15 kV for SEM analysis and two pictures were taken for each sample with different magnification. EDX analysis was run in conjunction with SEM analysis in order to measure the amount of count for elements within a chosen part of VPO particles and the result is shown as a text file.



**Figure 3.8: Hitachi S3400N**

### 3.3.3 Redox Titration

The acidic sites of the VPO catalysts are measured using potentiometric titration method, which was developed by Miki Niwa and Yuichi Murakami in 1982. The main focus of their research was to study the reaction mechanism of the ammoxidation of toluene on  $V_2O_5/Al_2O_3$  catalyst. The redox titration is carried out to determine the oxidation state of vanadium phase present in the doped catalyst, in order to obtain the average vanadium valence (AV) of VPO catalyst. Titration is generally out by means of glass electrode which is readily calibrated with standard buffer solutions. Also, the pH probe is used to measure the acid strength of the vanadium sample.

In this experimental study, a known amount of VPO catalyst was dissolved in 100 mL of sulphuric acid,  $H_2SO_4$ . The solution was firstly titrated with potassium permanganate,  $KMnO_4$  in order to eliminate the  $V^{3+}$  and  $V^{4+}$  phases by oxidising them to  $V^{5+}$  phase. End point was achieved when the colour of the solution changed from greenish blue to pink. The volume of  $KMnO_4$  used was recorded as  $V_1$ . The pink solution was then added with few drops of diphenylamine indicator,  $Ph_2NH$ . Next, the solution was treated with ammonium iron (II) sulphate solution,  $(NH_4)_2Fe(SO_4)_2$  to reduce  $V^{5+}$  to  $V^{4+}$ . The end point was determined when the colour of changed from

purple to colourless. The volume of ammonium iron (II) sulphate solution used was recorded as  $V_2$ .

Separately, another fresh 25 mL of the original solution was then titrated with ammonium iron (II) sulphate solution. Diphenylamine is also used as indicator. This stage of titration is act as reference sample, in order to determine the  $V^{5+}$  in the original solution. The end point is reached when the solution changes from purple to greenish blue. The volume of ammonium iron (II) sulphate solution used was recorded as  $V_3$ . The preparation of standard solution and procedure of running redox analysis is attached in Appendix D and E respectively. The respective concentration of the vanadium species in the catalyst can be determined by the following equation (Niwa & Murakami, 1982):-

$$(2V^{3+} + V^{4+})(V_a) = [MnO_4](V_2) \quad (3.3)$$

$$(V^{3+} + V^{4+} + V^{5+})(V_b) = [Fe^{2+}](V_2) \quad (3.4)$$

$$(V^{5+})(V_c) = [Fe^{2+}](V_3) \quad (3.5)$$

where

$V^{3+}$ ,  $V^{4+}$ ,  $V^{5+}$  = concentration of vanadium species at different oxidation state

$[MnO_4]$  = concentration of potassium permanganate

$[Fe^{2+}]$  = concentration of ammonium iron (II) sulphate solution

$V_1$  = volume of potassium permanganate used

$V_2$ ,  $V_3$  = volume of ammonium iron (II) sulphate solution used

$V_a$ ,  $V_b$ ,  $V_c$  = volume of the catalyst solution used

The average oxidation state of vanadium (AV) can be determined by solving the equation below:

$$V_{AV} = \frac{3V^{3+} + 4V^{4+} + 5V^{5+}}{V^{3+} + V^{4+} + V^{5+}} \quad (3.6)$$



**Figure 3.9: Redox Titration Method Setup**

### 3.3.4 Inductively Coupled Plasma – Optical Emission Spectroscopy (ICP-OES)

ICP-OES is commonly used instrument for analysis of trace elements in various fields. The sample is converted to excited atoms or ions by means of high plasma temperature. When an excited atom and ions relax to ground state, light is emitted producing line spectra in the UV-Vis regions (Robinson, 2005). The light emitted is generally associated with the element-unique wavelength and its respective intensity is proportional to the amount of that element present. Thus, by determining the wavelengths emitted and its intensity, we can identify the elements present in the sample using fingerprint matching with a reference standard, as well as its respective amount (Robinson, 2005).

OES can be used for the qualitative and quantitative identification of an element presents in the sample, even at low concentration (ppb) (Robinson, 2005). ICP is a type of plasma source in which the energy is supplied by electric current due to varying magnetic field. It significantly enhances the performance of OES, in which the high energy source can excite a wide range of elements, and yet produce very line-rich spectra (Robinson, 2005). In addition, the high temperature of plasma shows less matrix effect, by reducing chemical interference present in flame source OES.

Quantitative and qualitative analysis of the VPO catalysts were performed on a Perkin Elmer Emission Spectrometer Model Plasma 1000. To operate ICP-OES for catalyst samples, V and P calibration curve needs to be done first before calibrating the samples. Co calibration is also necessary as the samples are Co-doped. Sample introduced into the ICP as necessary to be in liquid form, hence VPO bulk catalyst samples were digested in 10 mL of HNO<sub>3</sub> to release the metal elements into solution for analysis in each dilution step. The prepared solution was then transferred into smaller test tubes and placed on the test tube stand. As shown in Figure 3.10, the sample is sucked into capillary tube by high pressure stream of Argon gas, breaking the liquid into a mist of fine particles. This process is known as nebulization. The aerosol particles is then transferred to plasma source, releasing the characteristic line spectra of analysed element.

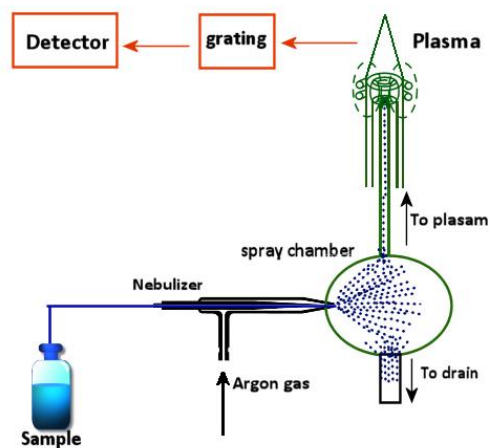


**Figure 3.10: Operating Mechanism of ICP-OES**

The multi elemental standards of the elements under research were prepared in the 3.125 to 50 ppm concentration range for vanadium, phosphorus and cobalt. The actual concentrations of the existing elements in the samples were determined from this range of standards using the calibration graphs obtained from the element standards. The preparation of standard solution and procedure of running ICP-OES analysis is attached in Appendix B and C respectively.



**Figure 3.11: Perkin Elmer Optical Emission Spectrometer Optima 7000 DV**

### 3.3.5 Temperature Programmed Reduction (TPR)

Temperature-programmed reduction (TPR) method was developed in which a heterogeneous catalyst is subjected to a flow of diluted hydrogen at ambient temperature. Hydrogen is being consumed as the catalyst is being reduced at increasing temperature. A thermal conductivity detector is used to measure the change in the thermal conductivity of the gas mixture before and after the reaction. The changes in conductivity are explained by the occurrence of reduction reaction on the catalysts' surface, in which each reduction reaction gives a peak shaped signal to the TPR curve. The software will interpret the data and provide information which is applicable to identify the number of reducible species present on the oxides' surface at most efficient reduction conditions.



**Figure 3.12: TPDRO Equipment**

In the TPR analysis, 0.02 g of catalyst was weighed into the reactor and connected to the preparation port. Pre-treatment process was carried out by flowing the 5.55 % of hydrogen in carrier nitrogen gas ( $\text{H}_2/\text{N}_2$ ) gas to remove the moisture from the sample. The catalyst was cleaned by heating it at  $10 \text{ K min}^{-1}$  from room temperature to 473 K in a purified nitrogen flow at  $25 \text{ cm}^3 \text{ min}^{-1}$ . The flow is maintained at 473 K for 30 minutes before cooling to ambient temperature. After which the flow is switched to 5.23 %  $\text{H}_2/\text{Ar}$  at  $25 \text{ cm}^3 \text{ min}^{-1}$ . The thermal conductivity

difference between the reactant and the carrier gas was optimized by the composition of the reducing gas. Temperature was raised at  $10 \text{ K min}^{-1}$  to  $1273 \text{ K}$  following the conductivity of the eluted gas. TPR profile is a plot of hydrogen consumption of a catalyst as a function of time, which is converted to a function of temperature.

## CHAPTER 4

## RESULTS AND DISCUSSION

## 4.1 X-Ray Diffraction (XRD)

The XRD spectrum of the precursor, as well as the Co-doped catalysts calcined at 700 °C in a reaction flow of nitrogen, i.e., 24 and 48 hours were presented in Figure 4.1.

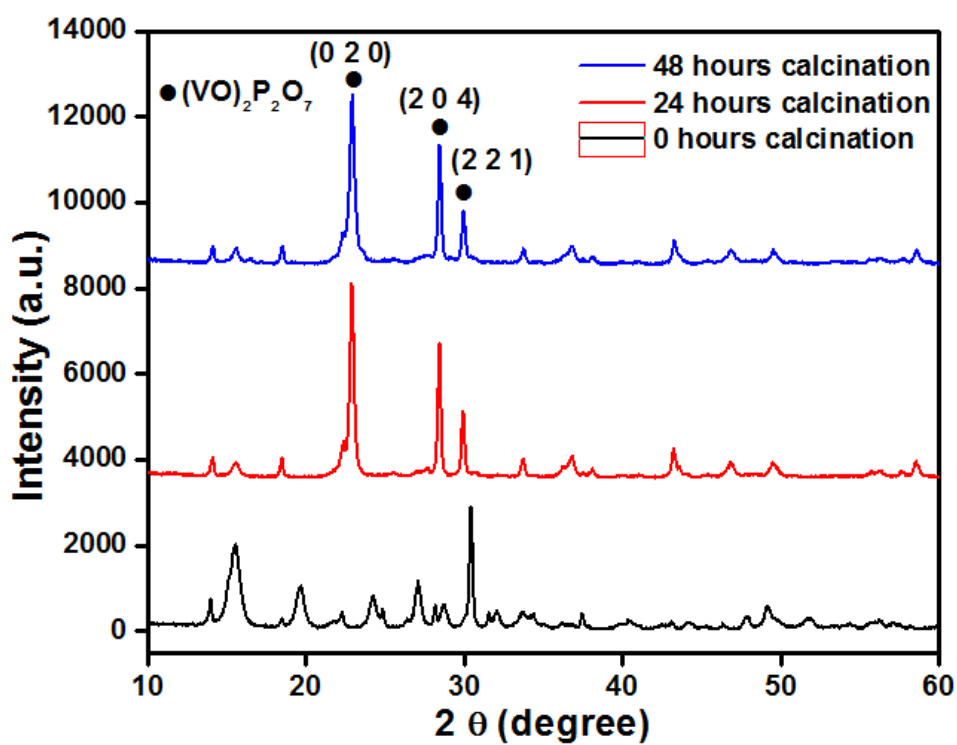


Figure 4.1: XRD Patterns of Precursor and Co-doped VPO Calcined at 24 and 48 hours

Inspection on the XRD spectrum of the precursor showed the presence of  $\text{VOHPO}_4 \cdot 1.5\text{H}_2\text{O}$ , which indicated from the 5 strongest peaks at  $2\theta = 15.5^\circ$ ,  $19.6^\circ$ ,  $24.2^\circ$ ,  $27.0^\circ$  and  $30.4^\circ$  (JCPDS File No. 37-0269). These peaks were in agreement of those reported by Ishimura et al. (2000), which indicated that the synthesis route for  $\text{VOHPO}_4 \cdot 1.5\text{H}_2\text{O}$  precursor was practical. It was crucial to identify the presence of these peaks as this may minimize the time spent on troubleshooting the similar characterization without realising the problems lie in the preparation of precursor.

For calcined samples, the intensities of the peaks concluded that these catalysts have a well crystallized  $(\text{VO})_2\text{P}_2\text{O}_7$  phase. The presence of  $(\text{VO})_2\text{P}_2\text{O}_7$  was recognised by the characteristic reflections with peaks at  $2\theta = 22.9^\circ$ ,  $28.4^\circ$  and  $29.9^\circ$  (JCPDS File No. 34-1381), which correspond to  $[0\ 2\ 0]$ ,  $[2\ 0\ 4]$  and  $[2\ 2\ 1]$  planes, respectively. In addition,  $\text{V}^{5+}$  phase species could be observed in the calcined sample, i.e.  $\beta\text{-VOPO}_4$  (JCPDS File No. 27-0948) observed at  $2\theta = 38.0^\circ$  for VPOCo-24. From the  $2\theta$  obtained, the crystallite size for each plane was calculated according to the  $2\theta$  obtained and tabulated in Table 4.1. Formula employed for this calculation is attached in Appendix F.

**Table 4.1: XRD Data on Cobalt-doped VPO Catalyst**

Catalyst	Line width	Line width ( $^\circ$ )	Crystallite Size	Crystallite Size
	( $^\circ$ ) $[0\ 2\ 0]$	$[2\ 0\ 4]$	( $\text{\AA}$ ) - $[0\ 2\ 0]$	( $\text{\AA}$ ) - $[2\ 0\ 4]$
VPOCo-24	0.32070	0.23950	249.7	338.2
VPOCo-48	0.38830	0.28100	206.3	288.3

As shown in Table 4.1, the FWHM of  $[0\ 2\ 0]$  and  $[2\ 0\ 4]$  planes were used to determine the crystallite size of the catalysts. The crystallite sizes of  $[0\ 2\ 0]$  plane for VPOCo-24 and VPOCo48 were 249.7  $\text{\AA}$  and 206.3  $\text{\AA}$  respectively, whereas the crystallite size of  $[2\ 0\ 4]$  plane for the same series were 338.2  $\text{\AA}$  and 288.3 $\text{\AA}$  respectively. According to Leong et al. (2012), the increased of calcination duration in 1% oxygen of nitrogen flow (1%  $\text{O}_2/\text{N}_2$ ) may result more intense major reflection peaks and narrower line width, which presents an enhanced formation of  $(\text{VO})_2\text{P}_2\text{O}_7$  phase. In addition, as calcination duration increased to 75 hours, the condition would enhance the formation of  $\text{V}^{5+}$  phase due to over oxidation. As shown in Table 4.1, prolong calcination duration in pure nitrogen flow tend to reduce the amount of

(VO)<sub>2</sub>P<sub>2</sub>O<sub>7</sub> phase, to be precise, degrading the crystallinity of VPO catalyst, however the formation of V<sup>5+</sup> was suppressed due to absence of oxygen in reaction flow. This was in agreement with the redox titration results, which showed that catalysts with longer activation duration do not yield any V<sup>5+</sup> phase.

Besides, the longer calcination duration tends to decrease the crystallite size of the VPOs catalysts prepared in [0 2 0] and [2 0 4] planes. With smaller crystallite size, it is predicted to exhibit larger specific surface area for VPOCo-48. This statement was in agreement with Wang et al. (1997), reported that higher amount of reduced species (V<sup>4+</sup>) yielded larger surface area, whereas the presence of V<sup>5+</sup> tends to cause crystallization that decreases the exposed area for catalytic reaction. As shown in the Figure 4.1, the VPOCo-48 showed higher abundance of V<sup>4+</sup> species than VPOCo-24, supporting that VPOCo-48 may exhibit higher specific surface area. The smaller crystallite size VPOCo-48 may contribute to higher specific surface area as well.

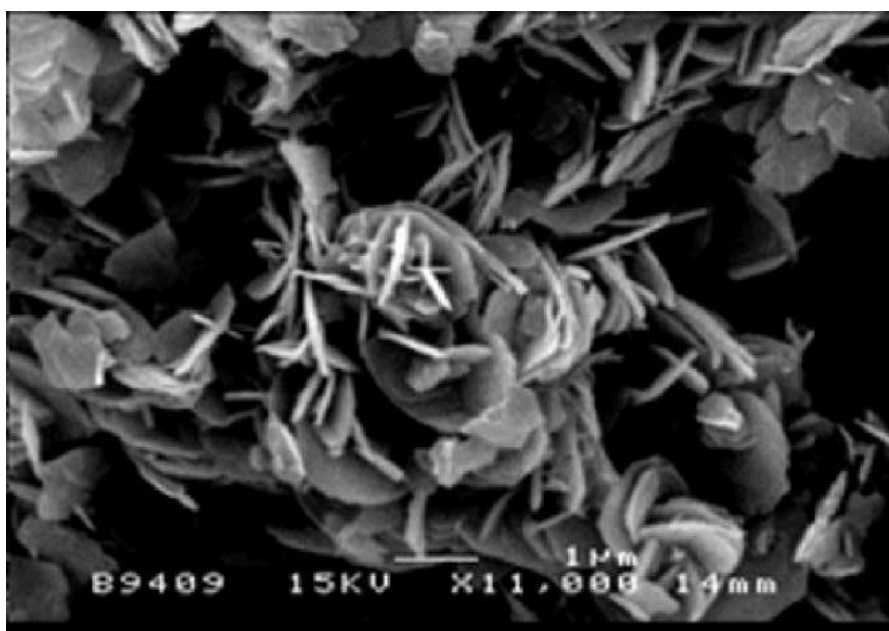
In short, it is shown that the addition of cobalt dopant does not improve the crystallinity of VPO catalyst desirably as the amount of (VO)<sub>2</sub>P<sub>2</sub>O<sub>7</sub> reduce, and acts as structural promoter that creates rougher and cracked crystal platelet as presented in SEM micrographs in the following section. This may lead to sintering of VPO catalyst in which crystallites may diffuse across the boundaries of particles in a Brownian-like motion, followed by subsequent nanoparticle growth due to coalescence (Dang et al., 2015). It is obvious that this may degenerate the active site available for catalytic reaction, but somehow reducing the amount of (VO)<sub>2</sub>P<sub>2</sub>O<sub>7</sub> phase, as well as the crystallinity of VPO sample. Thus, the parameter concerned in this technical report is to determine the optimum duration for the calcination to be carried out.

## 4.2 Scanning Electron Microscopy (SEM)

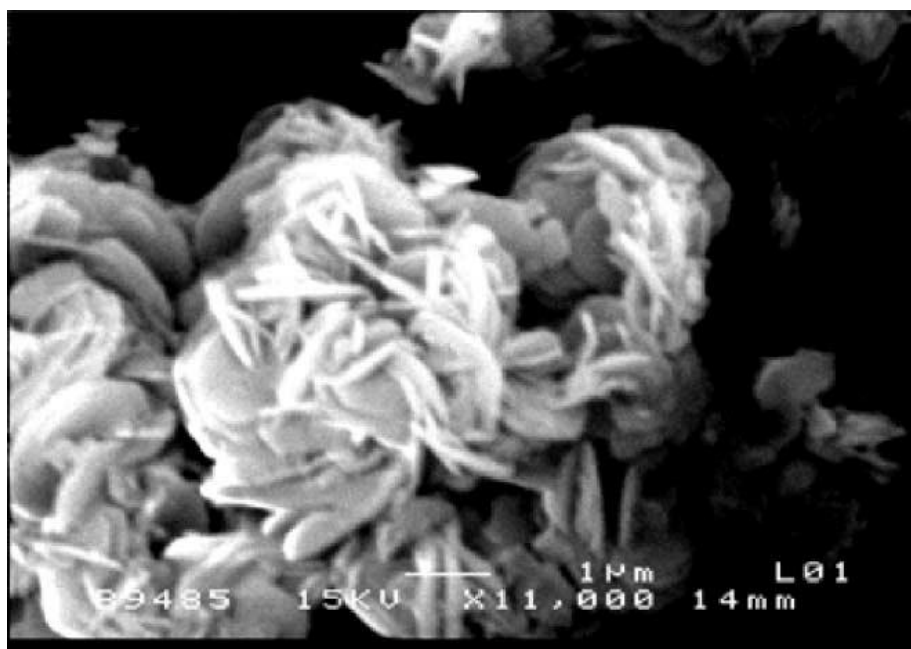
The surface morphologies of the VPO catalysts retrieved from the scanning electron microscopy with different calcinations duration and environment were presented in the following discussion. As discussed by Taufiq-Yap et al. (2001), the VPO catalyst prepared from sesquihydrate precursor, and calcined in 0.75% *n*-

butane/air presented an interesting feature, in which the platelets crystallite with folded edges agglomerated into rosette-shape clusters, as shown in Figure 4.2. As the calcination duration increased, there was consistent increase in the amount of rosette-shape clusters, and this phenomena encourages the clusters to agglomerate forming larger aggregates.

As the sesquihydrate precursor was subjected to 1% O<sub>2</sub>/N<sub>2</sub> flow environment, the result presented different surface morphology as shown in Figure 4.3, whereas cobalt-doped samples calcined in pure nitrogen flow were presented in Figure 4.4 and Figure 4.5. These catalysts showed different sizes of plate-like crystals with folded edges, which was similar to petals of rose flower (Leong et al., 2012). There was significant difference between undoped and doped VPO, in which the latter catalyst shows the presence of layered structure that sandwiched together due to intercalation due to inclusion of cobalt dopant into compound with VPO plate structure.

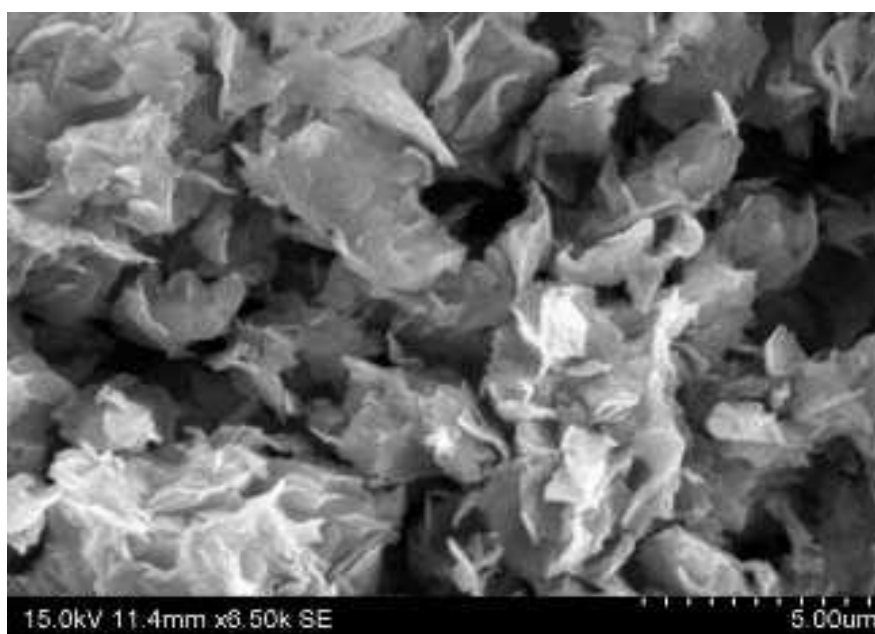


(a)

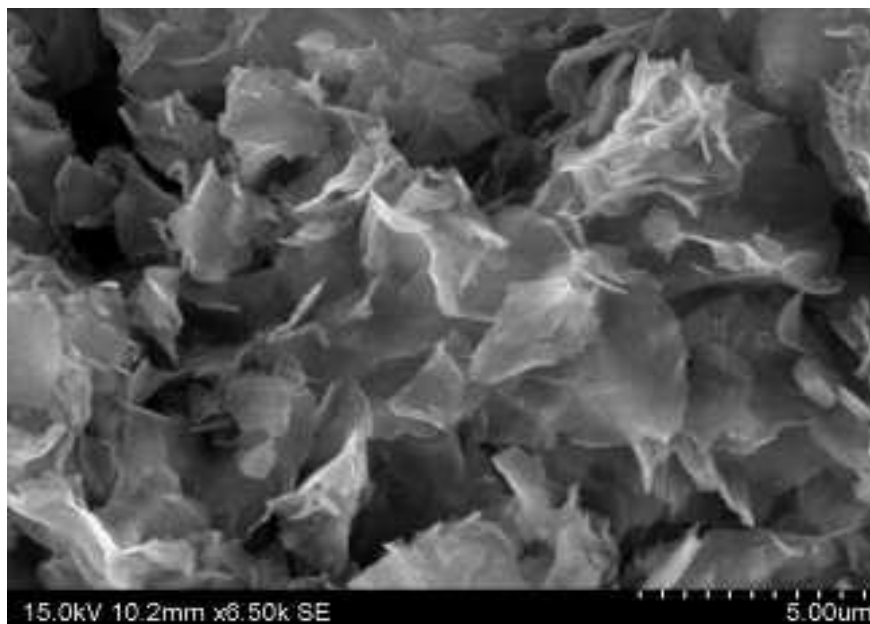


(b)

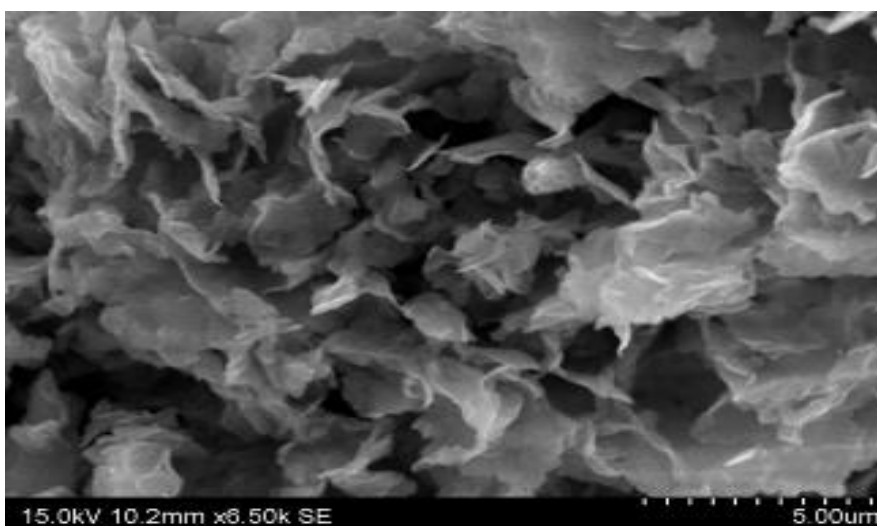
**Figure 4.2: SEM micrographs of VPO Catalyst in 0.75% *n*-butane/air for: (a) 24 hours; (b) 48 hours**



(a)



(b)

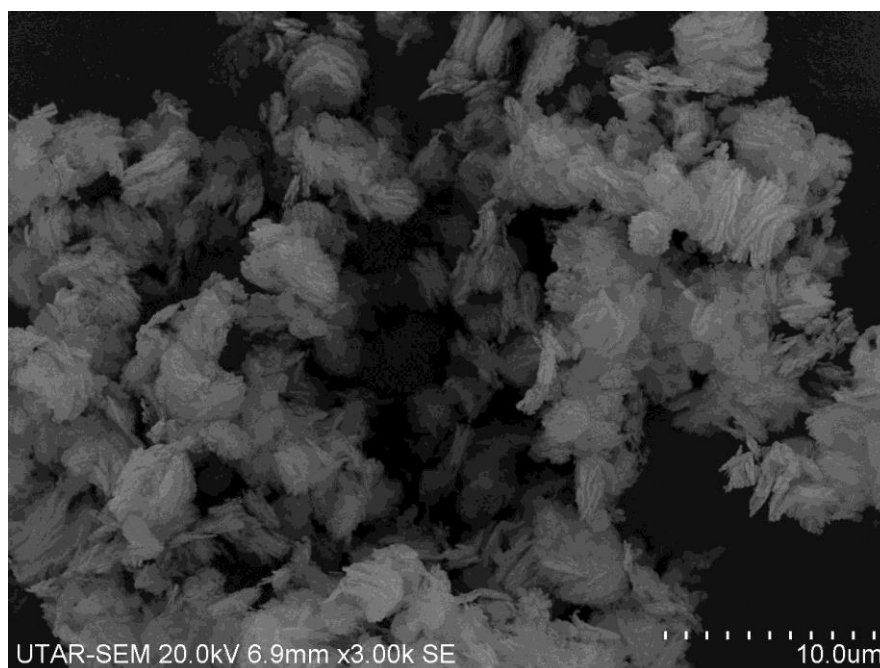


(c)

**Figure 4.3: SEM micrographs of VPO Catalyst in 1% O<sub>2</sub>/N<sub>2</sub> for: (a) 8 hours; (b) 16 hours; (c) 30 hours**

As the activation duration increased from 24 to 48 hours for cobalt doped VPO, it showed that the size of rough and cracked crystallite plate tends to decrease, which was in agreement with the result as discussed in XRD analysis. In addition, it was obvious that the particle of VPO catalyst in Figure 4.4 and 4.5 showed a well-crystallized layered structure due to the introduction of ultrasonic treatment during the synthesis of precursor.

As discussed in previous section, the microstructure, that is the shape and dimensions, of  $(VO)_2P_2O_7$  crystallites is generally considered to be a great influence on the catalyst's performance, hence it was a promising approach to modify the microstructure's shape and dimension in order to improve the catalytic performance of  $(VO)_2P_2O_7$  crystallites (Kamiya et al., 2006). Besides synthesizing the catalyst in relatively shorter time of 1 hr, ultrasonic treatment tends to enhance surface composition and better hydrocarbon oxidation activity compared with that prepared by conventional reflux method.

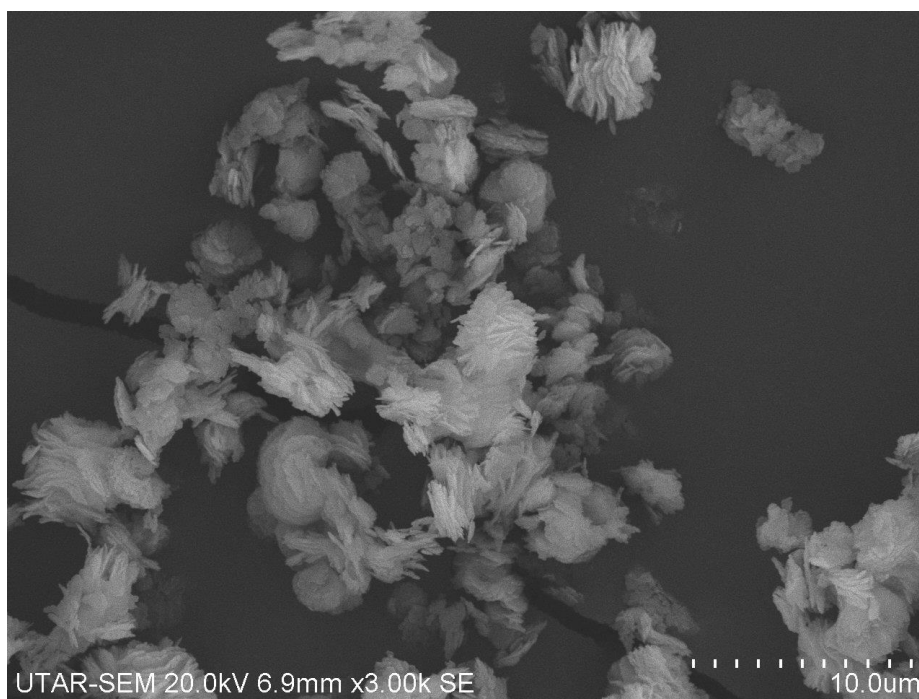


(a)

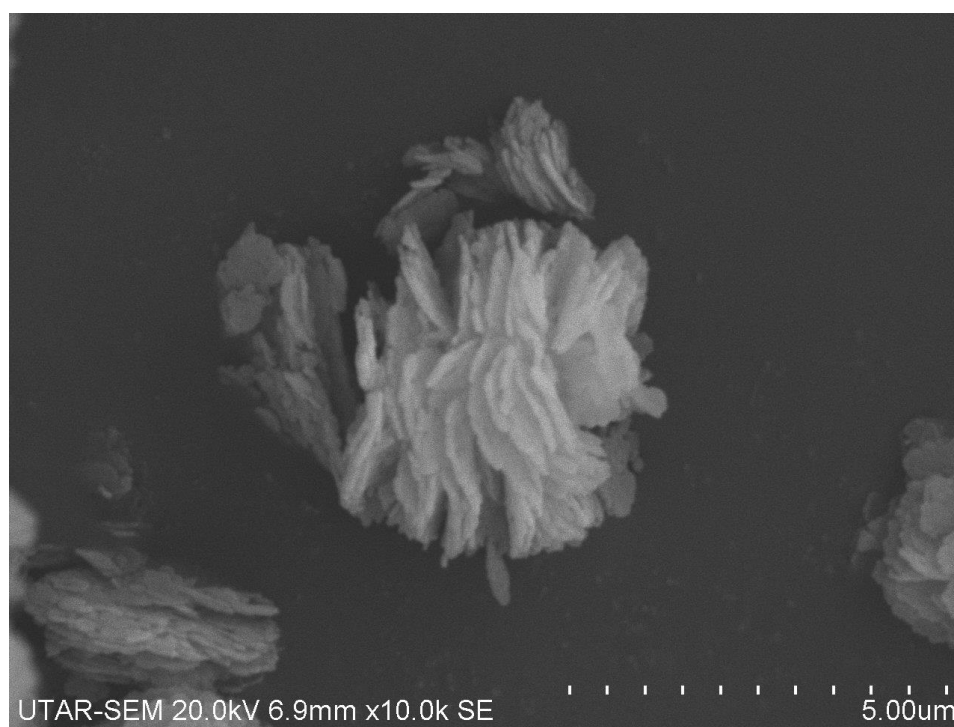


(b)

**Figure 4.4: SEM micrographs of Cobalt-doped VPO Catalyst in Nitrogen at (a) 3.0k and (b) 10.0k Magnification for 24 hours**



(a)



(b)

**Figure 4.5: SEM micrographs of Cobalt-doped VPO Catalyst in Nitrogen at (a) 3.0k and (b) 10.0k Magnification for 48 hours**

### 4.3 Energy Dispersive X-ray Spectrometer (EDX)

Generally, the P/V ratio and presence of elements in the catalyst can be identified via EDX technique as shown in Table 4.2. Since inhomogeneous and rough sample surface tends to reduce the accuracy of the sample, 3 points are selected in order to determine  $P_{ave}$  and  $V_{ave}$ , which are used to obtain the average P/V atomic ratio. In addition, the analysis can also be used to verify the presence of minute amount of cobalt in the catalyst, proving the dopant may incorporate into catalyst.

**Table 4.2: EDX Element Identification and Atomic P/V Ratio**

<b>Catalyst</b>	<b><math>P_{ave}</math> (At %)</b>	<b><math>V_{ave}</math> (At %)</b>	<b><math>O_{ave}</math> (At %)</b>	<b><math>Co_{ave}</math> (At %)</b>	<b><math>P/V_{ave}</math> Ratio</b>	<b><math>Co/V_{ave}</math> Ratio</b>
VPOCo-24	38.55	35.04	25.70	0.72	1.10	0.0205
VPOCo-48	36.46	37.55	24.04	0.62	0.97	0.0165

According to Gulianti (2005), an ideal catalyst composition was characterized by a slight excess of phosphate ( $P/V = 1.01-1.10$ ), with respect to empirical formula of  $VOHPO_4 \cdot 1.5H_2O$  precursor. An excess in phosphorus content may delay the oxidation of  $V^{4+}$  to  $V^{5+}$  and limit the over oxidation of the reduced vanadium species.

For EDX analyses, the P/V atomic ratio of VPOCo-24 and VPOCo-48 were 1.10 and 0.97 respectively as shown in Table 4.2, indicating a degrading trend for the catalyst performance. This could be explained that increase in activation duration tends to decrease the phosphorus content of the catalyst which is in agreement with the result deduced by Leong et al. (2012) for undoped VPO catalyst, ranging from 1.05 to 0.96. Hence, it is shown that the addition of cobalt dopant do not enhance the P/V ratio significantly.

However, the P/V and Co/V ratios for the synthesised catalyst do not rely solely on the result as expressed above because the analysis only focuses on surface instead of the overall bulk sample. Further clarification of catalyst compositions was conducted by ICP-OES and discussed in following section, especially for dopant concentration.

#### 4.4 Inductively Coupled Plasma – Optical Emission Spectroscopy (ICP-OES)

As discussed previously, the P/V atomic ratio and presence of dopant in the catalyst will be the parameter to be concerned under ICP-OES analysis, in which the result was presented in Table 4.3. Formula employed for this calculation was attached in Appendix G.

**Table 4.3: ICP-OES Element Identification and Atomic P/V Ratio**

<b>Catalyst</b>	<b>P<sub>ave</sub> (mg/L)</b>	<b>V<sub>ave</sub> (mg/L)</b>	<b>V<sub>ave</sub> (mol)</b>	<b>P/V<sub>ave</sub> Ratio</b>	<b>Co/V<sub>ave</sub> Ratio</b>
VPOCo-24	4.7830	8.9040	0.1240	0.8835	0.0120
VPOCo-48	1.9900	3.9240	0.0630	0.8341	0.0139

Based on the ICP-OES results, it was observed that as the calcination duration in pure nitrogen increases, the P/V atomic ratio showed a decreasing trend, from 0.8835 to 0.8341. The decreasing trend is in agreement with the result deduced from EDX analysis, as well as the result by Leong et al., (2012) for undoped catalyst in 1% O<sub>2</sub>/N<sub>2</sub> reaction flow, ranging from 1.24 to 0.86. However, the higher P/V ratio for undoped sample indicated that the presence of oxygen in the reaction flow tends to oxidise the reduced species from V<sup>4+</sup> to V<sup>5+</sup> phase.

In addition, the P/V atomic ratio for both doped samples were less than 1.0, comparing to optimum range being 1.01 to 1.10. According to Abon and Volta (1997), the P/V atomic ratio tend to be altered at the preparation stage and the activation condition may contribute to changes in the final phase composition and oxidation state distribution. It was crucial to determine P/V atomic ratio in order to limit high degree oxidation of (VO)<sub>2</sub>P<sub>2</sub>O<sub>7</sub> to V<sup>5+</sup> phase species. Even though certain level of V<sup>5+</sup> phase may contribute to higher selectivity, however it may suppress the activity of VPO catalyst at ratio beyond the optimum ranges (Taufiq-Yap and Saw, 2008).

Comparing the result from Table 4.2 and 4.3, P/V and Co/V ratios for EDX analysis were relatively higher than ICP-OES analysis due to the nature of analysis. Since EDX technique is classified as surface analysis, it allows higher amount of phosphorus and cobalt to be dispersed on sampling of catalyst, to be precise, enhancing the phosphorus surface enrichment resulting higher P/V and Co/V atomic ratio. However, the result from ICP-OES analysis represents the overall compositional ratio of the catalyst, as the measured values are based on the dissolved bulk catalyst.

#### **4.5 Redox Titration**

By conducting redox titration, the concentration of V<sup>4+</sup> and V<sup>5+</sup> phases in terms of percentage, as well as the average vanadium oxidation number was tabulated in Table 4.4. Formula employed for this calculation was attached in Appendix H.

**Table 4.4: Average Oxidation State of Vanadium**

Catalyst	V <sup>4+</sup> (%)	V <sup>5+</sup> (%)	V <sub>av</sub>
VOHPO <sub>4</sub> ·1.5H <sub>2</sub> O	100.00	0.00	4.0000
VPOCo-24	83.18	16.82	4.1682
VPOCo-48	100.00	0.00	4.0000

As shown in Table 4.4, the average oxidation state of vanadium for precursor, VPOCo-24 and VPOCo-48 were 4.0000, 4.1682 and 4.0000 respectively. Under pure nitrogen calcination environment, the precursor experienced topotactic transformation, involved a structural change from VOHPO<sub>4</sub>·1.5H<sub>2</sub>O to (VO)<sub>2</sub>P<sub>2</sub>O<sub>7</sub> crystalline solids. This can be proven due to presence of V<sup>5+</sup> phase, from 0% to 16.82%, supported with the XRD pattern shown in previous section. As the calcination duration increased to 48 hours, it tend to suppress the formation of V<sup>5+</sup> phase, in short, it concluded that the VPOCo-24 displayed higher selectivity for MA than VPOCo-48 due to fair level of V<sup>5+</sup>. This is agreeable with the findings of Guliants and Carreon (2005), since the VPOs catalyst characterized with a high V<sup>5+</sup> content have higher selectivity with lower activity.

However, presented by Leong et al. (2012), as the precursor was subjected to 1% O<sub>2</sub>/N<sub>2</sub> calcination environment, the calcined undoped sample showed a higher average oxidation state of vanadium compared to result shown in Table 4.4. As the calcination duration increased, the percentage of V<sup>5+</sup> phase increased significantly from 21% to 50%. The increment trend in undoped sample was generally due to oxidation of reduced species in the presence of oxygen in the reaction flow, even though in minute concentration.

In addition, it can explained by the fact discussed by Cornogalia et al. (2003) stated the presence of cobalt enhances surface phosphorus enrichment, hence limiting the oxidation of reduced species. This is in agreement with the result shown in Table 4.4, as the percentage of V<sup>5+</sup> for cobalt-doped sample was significantly lower compared to the undoped sample in the discussion by Leong et al. (2012).

#### 4.6 Temperature Programmed Reduction (TPR)

Temperature Programmed Reduction (TPR in  $H_2$ ) is used to investigate redox properties of the catalyst. An oxidized catalyst was submitted to programmed temperature rise in a flow of reducing gas mixture, generally hydrogen diluted in inert nitrogen or argon. Figure 4.6 shows the TPR profile of VPO in  $H_2/N_2$  (5.47 %  $H_2$  in  $N_2$ , 1000 Pa, and  $25\text{ cm}^3\text{min}^{-1}$ ), when subjected to programmed temperature rise from ambient to 1273K at  $10\text{ Kmin}^{-1}$  in the reducing flow. Figure 4.6 shows the TPR profile for the inspected samples, while Table 4.5 lists the peaks maximum temperatures, reduction activation energy, the amount of oxygen in each peak respectively.

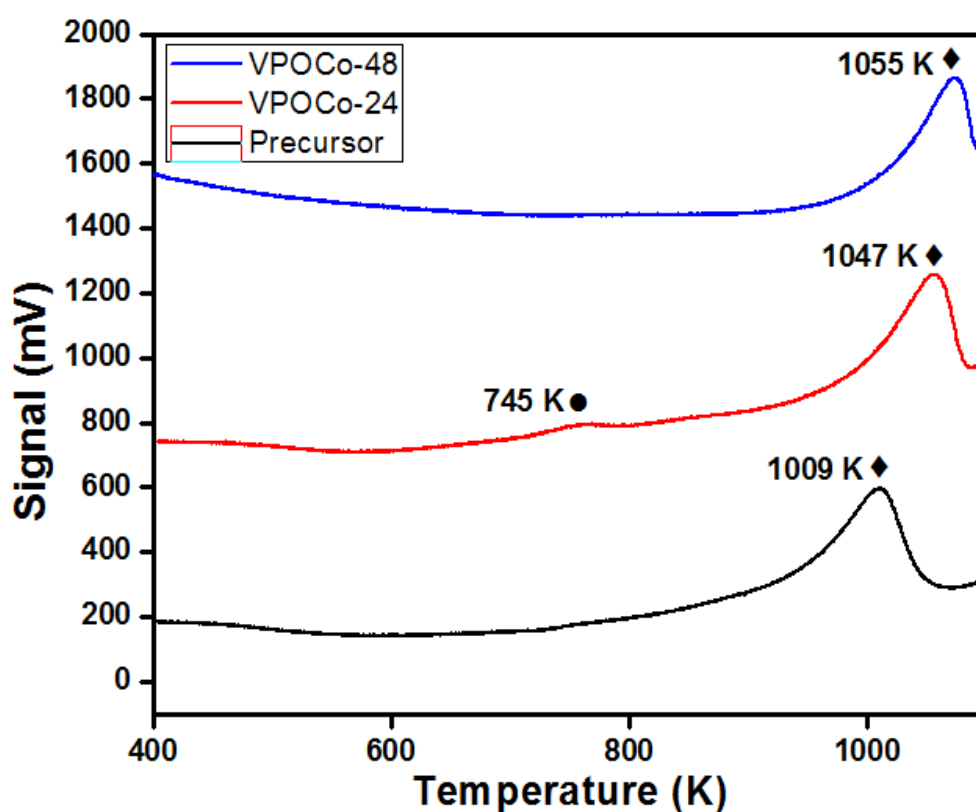


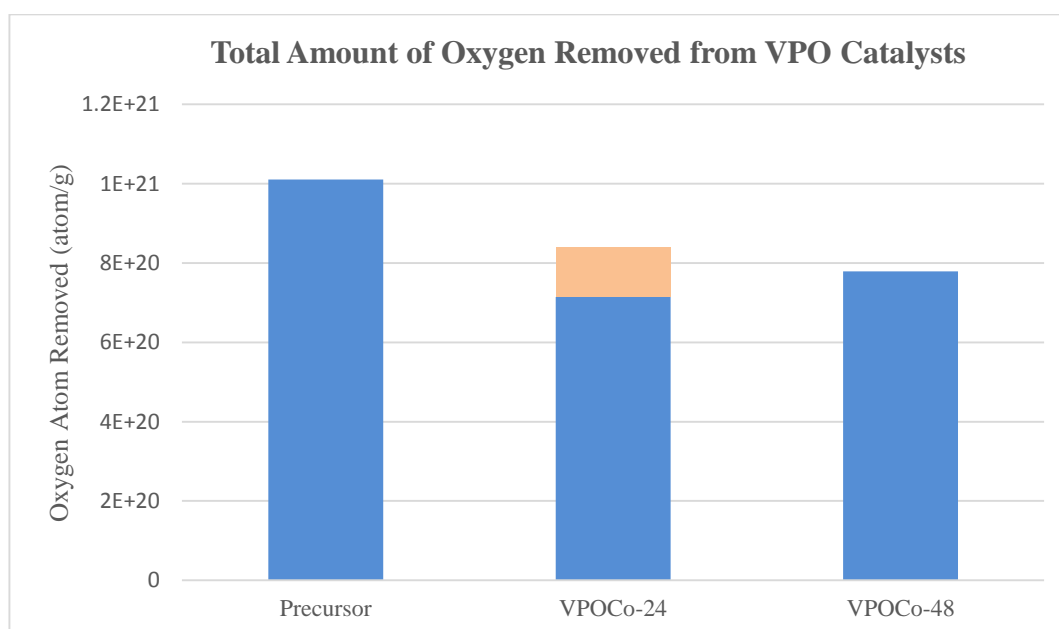
Figure 4.6: TPR in  $H_2/N_2$  profiles for VPOs catalysts

**Table 4.5: Total number of oxygen atoms removed from catalyst by reduction in H<sub>2</sub>/N<sub>2</sub>**

Sample	Temperature Maxima, T <sub>m</sub> (K)	Reduction Activation Energy, E <sub>r</sub> (kJmol <sup>-1</sup> )	Amount of oxygen removed (mol/g)	Amount of oxygen removed (atom/g)
VOHPO <sub>4</sub> ·1.5H <sub>2</sub> O	1009	168.74	1.677×10 <sup>-3</sup>	1.010×10 <sup>21</sup>
<b>TOTAL</b>			1.677×10 <sup>-3</sup>	1.010×10 <sup>21</sup>
VPOCo-24	745	124.59	2.093×10 <sup>-4</sup>	1.260×10 <sup>20</sup>
	1047	175.09	1.186×10 <sup>-3</sup>	7.142×10 <sup>20</sup>
<b>TOTAL</b>			1.395×10 <sup>-3</sup>	8.403×10 <sup>20</sup>
VPOCo-48	1055	176.43	1.293×10 <sup>-3</sup>	7.787×10 <sup>20</sup>
<b>TOTAL</b>			1.293×10 <sup>-3</sup>	7.787×10 <sup>21</sup>

A few important points were highlighted in the TPR profiles. All the catalyst gave major peak maxima at 1009K, 1047K and 1055K for VOHPO<sub>4</sub>·1.5H<sub>2</sub>O, VPOCo-24 and VPOCo-48 respectively. These peak was assigned to removal of the lattice oxygen O<sup>-</sup> from the active V<sup>4+</sup> phase. In addition, for VPOCo-24, it gave a peak at 745 K, corresponded to the removal of O<sup>2-</sup> from V<sup>5+</sup> phase (Goh et al., 2008).

**Figure 4.7: Data Chart of TPR in H<sub>2</sub>/N<sub>2</sub> for bulk VPO Catalyst**



As shown in Figure 4.7, for VPOCo-24, about 13.57 % of oxygen was removed from  $V^{5+}$  for VPOCo-24, which was in agreement with the result from redox titration, in which the catalyst comprises 10.75% of  $V^{5+}$  phase. In addition, the amount of oxygen removed from  $V^{4+}$  for VPOCo-48 is higher than VPOCo-24, which supported that it exhibited higher surface area in the previous section.

Supported by Leong et al. (2012), increasing the activation duration shifted the reduction peak to higher temperature. However, the amount of oxygen removed from the undoped catalyst in 1%  $N_2/O_2$  was higher, ranging from  $1.58 \times 10^{21}$  to  $2.57 \times 10^{21}$  atoms/g. Thus, it can be concluded that the addition of cobalt dopant would create layered structure as shown in SEM micrographs, which may lead to enhancement of the amount of oxygen species removed due to larger specific surface area as compared to undoped VPO catalyst.

## CHAPTER 5

### CONCLUSION AND RECOMMENDATIONS

#### 5.1 Conclusion

Vanadium phosphate catalysts were prepared by calcining  $\text{VOHPO}_4 \cdot 1.5\text{H}_2\text{O}$  for different duration (24 and 48 hours) under pure nitrogen flow, in order to create anaerobic atmosphere. The synthesis of sesquihydrate precursor involved a two-step procedure in which  $\text{VOPO}_4 \cdot 2\text{H}_2\text{O}$  acted as an intermediate before obtaining the precursor. Interestingly, it enhanced the formation of  $\text{V}^{5+}$  phase in the catalysts.

Activation duration affects the morphology of the catalyst. Results from XRD analysis had shown the crystalline sizes decreased under prolong calcination duration, which lead to increment in specific surface area. Scanning electron microscopy clearly showed that catalysts exhibited plate-like crystallites with folded edges, which were similar to petals of flowers that sandwiched together in layered structure. For EDX and ICP, both results presented similar trend, in which the P/V atomic ratio decreased as calcination duration increased. Prolong the duration of  $\text{N}_2$  calcination also resulted in an increment in the amount of oxygen desorbed from  $\text{V}^{4+}$  species. Lastly, as shown in redox titration and TPR analysis, the VPOCo-24 exhibited higher selectivity than VPOCo-48, due to the fair level of  $\text{V}^{5+}$  phase in the catalyst.

In addition, the addition of cobalt dopant acted as structural promoter that created rougher and cracked crystal platelet as observed in the SEM micrographs. The layered structure exhibited higher specific surface area compared to undoped sample, which was supported by comparing the amount of oxygen removed in TPR analysis

with results from Leong et al. (2012). The presence of cobalt limited the oxidation of reduced species, produced catalyst with higher activity. Lastly, in order to produce catalyst that yield higher specific surface area and activity, the doped precursor should be subjected to 48 hours calcination duration under pure nitrogen flow.

## **5.2 Recommendations**

For further research:

1. Catalyst produced should be tested using the catalytic reactor which would yield the selectivity of the catalyst towards maleic anhydride formation and activity toward n-butane conversion. These data as crucial as they play an important role in determining the optimal catalyst.
2. Various dopants can be added so that the effect of doping towards the physical, chemical, reactivity and catalytic properties of the doped VPOs catalyst can be studied.
3. Catalyst should be prepared via microwave irradiation for both first and second stage implying the sesquihydrate route and the result obtained compared between organic and hemihydrate route to distinguish a better and newer way of producing catalyst.

## REFERENCES

- Abon, M., Volta, J.C. (1997). Vanadium phosphorus oxides for n-butane oxidation to maleic anhydride. *Applied Catalysis A: General* **157**: 173~193.
- Abon, M., Bere, K.E., Tuel, A., and Delichere, P. (1995). Evolution of a VPO Catalyst in n-Butane Oxidation Reaction during the Activation Time. *Journal of Catalysis* **156**: 28-36.
- Arquimedes, C.-L., Guilhaume, N., Miachon, S., and Dalmon, J.-A. (2005). Selective oxidation of butane to maleic anhydride in a catalytic membrane reactor adapted to rich butane feed. *Catalysis Today* **107-108**: 949-956.
- Casaletto, M.P., Lisi, L., Mattogno, G., Patrono, P., and Ruoppolo, G. (2003). Effect of the support on the surface composition of vanadium phosphate catalysts in the oxidative dehydrogenation of ethane. *Surf. Interface Anal.* 2004; **36**: 737–740.
- Centi, G., & Trifiro, F. (1990). *New developments in selective oxidation*. Elsevier Science Publication.
- Centi, G., Trifiro, F., Ebner, J. R., & Franchetti, V. M. (1988). Mechanistic aspects of maleic anhydride synthesis from C4 hydrocarbon over phosphorus vanadium oxide. *Chem. Rev.*, 88(1), 55-80.
- Chorkendorff, I., & Niemantsverdriet, J. W. (2003). *Concept of modern catalysis and kinetics*. Wiley-Interscience: John Wiley & Sons Inc.
- Cornaglia, L., Irusta, S., Lombardo, E. A., Durupty, M. C., and Volta, J. C. (2003). The beneficial effect of cobalt on VPO catalysts. *Catalysis today* **78**: 291-301.

Feng, R.-M., Yang, X.-J., Ji, W.-J., Chen, Y., and Au, C.-T. (2007). VPO catalysts supported on H<sub>3</sub>PO<sub>4</sub>-treated ZrO<sub>2</sub> highly active for *n*-butane oxidation. *Journal of Catalysis* **246**: 166-176.

Felthouse, T. R., Burnett, J. C., Horrell, B., Mummey, M. J., & Kou, Y. J. (2001). *Maleic anhydride, maleic acid and fumaric acid*. Retrieved from <http://www.southalabama.edu/chemistry/barletta/felthouse.pdf> on 18th August 2015.

Goh, C.K., Taufiq-Yap, Y.H., Hutchings, G.J., Dummer, N., Bartley, J., (2008). Influence of Bi-Fe additives on properties of vanadium phosphate catalysts for *n*-butane oxidation to maleic anhydride. *Catalysis Today* **131**, 408-412.

Govender, N., Friedrich, H.B., Matthys Janse, V.V. (2004). Controlling factors in the selective conversion of *n*-butane over promoted VPO catalysts at low temperature. *Catalysis Today* **97**: 315-324.

Gulians, V.V., Carreon, M.A. (2005) Vanadium-Phosphorus-Oxides: from Fundamentals of *n*-Butane Oxidation to Synthesis of New Phases. *Catalysis, Volume 18*.

Gulians, V.V. (1999). Structure-reactivity relationships in oxidation of C<sub>4</sub> hydrocarbons on supported vanadia catalysts. *Catalysis Today* **51**: 255-268.

Huang, X. F., Chen, B. H., Liu, B. J., Silveston, P. L., & Li, C. Y. (2002). *Reoxidation kinetics of a VPO catalyst*. *Catalysis Today*, 74(1-2), 121-130

Ishimura, T., Sugiyama, S., and Hayashi, H. (2000). Vanadyl hydrogenphosphate sesquihydrate as a precursor for preparation of (VO)<sub>2</sub>P<sub>2</sub>O<sub>7</sub> and cobalt-incorporate catalysts. *Journal of Molecular Catalysis A-Chemical*, Vol.158, No.2, 559-565.

Leong, L.K. and Thang L.Y. (2012). *Effect of activation duration in 1% oxygen in nitrogen balance on vanadium phosphate catalysts synthesized via sesquihydrate route*. Retrieved from on 16th March 2016.

Mahony, L.O., Henry, J., Sutton, D., Curtin, T., Hodnett, B.K. (2003). Crystallisation of  $\text{VOHPO}_4 \cdot 0.5\text{H}_2\text{O}$ . *Applied Catalysis A: General* **253**:409-416.

Narayana, K.V., Martin, A., Lucke, B., Belmans, M., Boers, F., and Van Deynse, D. (2005). Preparation, Solid-state Characteristics, and Catalytic Properties of Promoted Vanadium Phosphate Materials. *Z. Anorg. Allg. Chem.*, **631**, 25-30.

Patience, G.S., Bockrath, R.E., Sullivan, J.D., and Horowitz, H.S. (2007). Pressure Calcination of VPO Catalyst. *Ind. Eng. Chem. Res.*, **46** (13), 4374-4381.

Perego, G.G. (1998). Characterization of heterogeneous catalysts by X-ray diffraction techniques. *Catalysis Today* **41**, 251-259.

Pierini, B.T., and Lombardo, E.A. (2005). Structure and properties of Cr promoted VPO catalysts. *Materials Chemistry and Physics* **92**: 197–204.

Rownaghi, A.A., Taufiq-Yap, Y.H., Rezaei, F. (2009). Solvothermal synthesis of vanadium phosphate catalysts for n-butane oxidation. *Chemical Engineering Journal* **155**: 514-522.

Spivey, J., Gulians, V.V., & Carreon, M. (2005). Vanadium-phosphorus-oxides: From fundamentals of n-butane oxidation to synthesis of new phases. In *Catalysis* (p. 1- 45). UK: RSC Publishing.

Taufiq-Yap, Y. H., Looi, M., Wong, Y., & Hussien, M. Z. (2001). Physico- chemical characterization of vanadium phosphorus-oxide catalyst prepared in organic and aqueous medium. *Jurnal Teknologi*, 34(C), 17-24.

Taufiq-Yap, Y.H., Leong, L.K., Hussein, M.Z., Irmawati, R., and Abd Hamid, S.B. (2004). Synthesis and characterisation of vanadyl pyrophosphate catalysts via vanadyl hydrogen phosphate sesquihydrate precursor. *Catalysis Today* **93-95**:715-722.

Taufiq-Yap, Y. H., Goh, C. K., Hutchings, G. J., Dummer, N., & Bartley, J. K. (2006). Effect of mechanochemical treatment to the vanadium phosphate catalysts derived from  $\text{VOPO}_4 \cdot 2\text{H}_2\text{O}$ . *Journal of Molecular Catalysis*, 260(1-2), 24-31.

Taufiq Yap, Y. H., Rownanghi. A. A., Hussien, M. Z. & Irmawati, R. (2007). Preparation of vanadium phosphate catalyst from  $\text{VOPO}_4 \cdot 2\text{H}_2\text{O}$ : Effect of microwave irradiation on morphology and catalytic property. *Catalyst Letter*, 119, 64-71.

Taufiq-Yap, Y.H., Saw, C.S. (2008). Effect of different calcination environments on the vanadium phosphate catalysts for selective oxidation of propane and *n*-butane. *Catalysis Today* **131:285-291**.

Waugh, K.C., and Taufiq-Yap, Y.-H. (2003). The effect of varying the duration of the butane/air pretreatment on the morphology and reactivity of  $(\text{VO})_2\text{P}_2\text{O}_7$  catalysts. *Catalysis Today* **81: 215-225**.

Xiao, C.Y., Chen, X., Wang, Z.Y., Ji, W.J., Chen, Y., and Au, C.T. (2004). The novel and highly selective fumed silica-supported VPO for partial oxidation of *n*-butane to maleic anhydride. *Catalysis Today* **93-95: 223-228**.

Zazhigalov, V.A., Bacherikova, I.V., Stokh, E., Komashko, G.A., and Pyatnitskaya, A.I. (1994). Mechanism of the effect of alkali and alkaline-earth element additives on the properties of V-P-O catalysts of oxidation of *n*-butane. *Theoretical and Experimental Chemistry*, Vol. 30, No.2.

## APPENDICES

### APPENDIX A: Dopant Calculation

**1. Determine the molecular weight of VOPO<sub>4</sub>·2H<sub>2</sub>O and dopant Co(NO<sub>3</sub>)<sub>2</sub>**

From Periodic Table:

H = 1.00794 g/mole	V = 50.9415 g/mole
O = 15.9994 g/mole	N = 14.0064 g/mole
P = 30.9738 g/mole	Co = 58.9332 g/mole

**Vanadyl Phosphate Dihydrate: VOPO<sub>4</sub>·2H<sub>2</sub>O**

$$\begin{aligned} \text{Molecular weight of VOPO}_4 \cdot 2\text{H}_2\text{O} &= [(50.9415) + (15.9994) + (30.9738) + \\ &4(15.9994) + 2[2(1.00794) + (15.9994)]] \\ &= \mathbf{197.9428 \text{ g/mole}} \end{aligned}$$

**Dopant: Co(NO<sub>3</sub>)<sub>2</sub>**

$$\begin{aligned} \text{Molecular weight of Co(NO}_3)_2 &= [(58.9332) + 2[(14.0064) + 3(15.9994)]] \\ &= \mathbf{182.8924 \text{ g/mole}} \end{aligned}$$

**2. Determine the molarity of VOPO<sub>4</sub>·2H<sub>2</sub>O**

Dopants are added based on 10.0 g of VOPO<sub>4</sub>·2H<sub>2</sub>O

Thus, for 10.0 g of VOPO<sub>4</sub>·2H<sub>2</sub>O, the molarity is computed.

Molarity of VOPO<sub>4</sub>·2H<sub>2</sub>O

$$= \frac{10 \text{ g}}{197.9428 \text{ g/mole}} = \mathbf{0.0505 \text{ mole}}$$

**3. Determine the amounts of dopant needed**

For Co 1 %

Molarity of  $\text{Co}(\text{NO}_3)_2$

$$= 0.0505 \times 1\% = \mathbf{0.000505 \text{ mole}}$$

Weight of  $\text{Co}(\text{NO}_3)_2$

$$= 0.000505 \text{ mol} \times 182.8924 \text{ gmol}^{-1} = \mathbf{0.0924 \text{ g}}$$

## APPENDIX B: Preparation of Solutions Used in ICP-OES

**i. Preparation of 8M HNO<sub>3</sub>**

Molarity for 65% of HNO<sub>3</sub>

$$= \frac{\text{Density of HNO}_3}{\text{Molecular Weight of HNO}_3} \times \frac{65}{100} \times 1000$$

$$= \frac{1.4090 \text{ gcm}^{-3}}{63.0130 \text{ gmol}^{-1}} \times \frac{65}{100} \times 1000 = 14.53 \text{ molL}^{-1} = 14.53 \text{ M}$$

$$M_1V_1 = M_2V_2$$

where,

$$M_1 = \text{Concentration of 65\% of HNO}_3 (14.5343 \text{ M})$$

$$V_1 = \text{Volume of 65\% of HNO}_3$$

$$M_2 = \text{Concentration of 8 M HNO}_3$$

$$V_2 = \text{Volume of 8 M HNO}_3$$

$$M_1V_1 = M_2V_2$$

$$(14.53 \text{ M})V_1 = (8 \text{ M})(1000 \text{ mL})$$

$$V_1 = 550 \text{ mL}$$

Thus, 550 mL of 65 % of HNO<sub>3</sub> was diluted to 1000 mL volumetric flask with deionised water.

## ii. Preparation of Stock Solution of Phosphorus, P

Molecular weight of  $\text{NH}_4\text{H}_2\text{PO}_4$

$$= 14.0067 + 6(1.0079) + 30.9738 + 4(15.9994)$$

$$= 115.0255 \text{ g mol}^{-1}$$

$$50 \text{ ppm of stock solution for P} = 50 \text{ mg L}^{-1} = 0.05 \text{ g L}^{-1}$$

Number of mole of P

$$= \frac{0.05 \text{ gL}^{-1}}{30.9738 \text{ gmol}^{-1}} = 0.001614 \text{ molL}^{-1}$$

Mass of  $\text{NH}_4\text{H}_2\text{PO}_4$

$$= 0.001614 \text{ molL}^{-1} \times 115.0255 \text{ gmol}^{-1} = 0.1857 \text{ gL}^{-1}$$

Thus, 0.1857 g of  $\text{NH}_4\text{H}_2\text{PO}_4$  was transferred into 1000 mL volumetric flask and top up with deionised water.

### Preparation of standard solution of phosphorus, P

$$M_1V_1 = M_2V_2$$

where,

$$M_1 = \text{Concentration of stock solution (50 ppm)}$$

$$V_1 = \text{Volume of stock solution}$$

$$M_2 = \text{Concentration of standard solution}$$

$$V_2 = \text{Volume of standard solution}$$

### Example of calculation for standard solution of 25 ppm

$$M_1V_1 = M_2V_2$$

$$(50\text{ppm})V_1 = (25\text{ppm})(100 \text{ mL})$$

$$V_1 = 50 \text{ mL}$$

Thus, 50 mL of stock solution for phosphorus was dissolved in 8 M  $\text{HNO}_3$  then diluted to 100 mL with deionised water to produce 25 ppm standard solution of phosphorus.

### iii. Preparation of Stock Solution of Vanadium, V

Molecular weight of  $\text{NH}_4\text{VO}_3$

$$= 14.0067 + 4(1.0079) + 50.9415 + 3(15.9994)$$

$$= 116.9780 \text{ g mol}^{-1}$$

$$50 \text{ ppm of stock solution for P} = 50 \text{ mg L}^{-1} = 0.05 \text{ g L}^{-1}$$

Number of mole of P

$$= \frac{0.05 \text{ gL}^{-1}}{50.9415 \text{ gmol}^{-1}} = 0.0009815 \text{ molL}^{-1}$$

Mass of  $\text{NH}_4\text{VO}_3$

$$= 0.0009815 \text{ molL}^{-1} \times 116.9780 \text{ gmol}^{-1} = 0.1148 \text{ gL}^{-1}$$

Thus, 0.1148 g of  $\text{NH}_4\text{VO}_3$  was transferred into 1000 mL volumetric flask and top up with deionised water.

#### Preparation of standard solution of vanadium, V

$$M_1V_1 = M_2V_2$$

where,

$$M_1 = \text{Concentration of stock solution (50 ppm)}$$

$$V_1 = \text{Volume of stock solution}$$

$$M_2 = \text{Concentration of standard solution}$$

$$V_2 = \text{Volume of standard solution}$$

#### Example of calculation for standard solution of 25 ppm

$$M_1V_1 = M_2V_2$$

$$(50\text{ppm})V_1 = (25\text{ppm})(100 \text{ mL})$$

$$V_1 = 50 \text{ mL}$$

Thus, 50 mL of stock solution for phosphorus was dissolved in 8 M  $\text{HNO}_3$  then diluted to 100 mL with deionised water to produce 25 ppm standard solution of vanadium.

#### iv. Preparation of Stock Solution of Cobalt (Co)

$$\begin{aligned} &\text{Molecular weight of Co(NO}_3)_2 \\ &= 58.9332 + 2[14.0067 + 3(15.9994)] \\ &= 183.9430 \text{ g mol}^{-1} \end{aligned}$$

$$50 \text{ ppm of stock solution for P} = 50 \text{ mg L}^{-1} = 0.05 \text{ g L}^{-1}$$

$$\begin{aligned} &\text{Number of mole of P} \\ &= \frac{0.05 \text{ gL}^{-1}}{183.9430 \text{ gmol}^{-1}} = 0.0002719 \text{ molL}^{-1} \end{aligned}$$

$$\begin{aligned} &\text{Mass of NH}_4\text{VO}_3 \\ &= 0.0002719 \text{ molL}^{-1} \times 183.9430 \text{ gmol}^{-1} = 0.0498 \text{ gL}^{-1} \end{aligned}$$

Thus, 0.1561 g of  $\text{Co(NO}_3)_2$  was transferred into 1000 mL volumetric flask and top up with deionised water.

#### Preparation of standard solution of cobalt, Co

$$M_1V_1 = M_2V_2$$

where,

$$M_1 = \text{Concentration of stock solution (50 ppm)}$$

$$V_1 = \text{Volume of stock solution}$$

$$M_2 = \text{Concentration of standard solution}$$

$$V_2 = \text{Volume of standard solution}$$

#### Example of calculation for standard solution of 5 ppm

$$M_1V_1 = M_2V_2$$

$$(50\text{ppm})V_1 = (5\text{ppm})(100 \text{ mL})$$

$$V_1 = 10 \text{ mL}$$

Thus, 10 mL of stock solution for phosphorus was dissolved in 8 M  $\text{HNO}_3$  then diluted to 100 mL with deionised water to produce 5 ppm standard solution of cobalt.

**v. Preparation of 100 ppm sample solution**

$$\begin{aligned} 0.01 \text{ g sample in } 100 \text{ mL} &= \frac{0.01 \text{ g}}{100 \text{ mL HNO}_3} \\ &= \frac{10 \text{ mg}}{0.1 \text{ L HNO}_3} = 100 \text{ mgL}^{-1} \\ &= 100 \text{ ppm} \end{aligned}$$

Thus, 0.01 g of sample was dissolved in 100 mL of 8 M HNO<sub>3</sub> to produce 100 ppm sample solution.

## APPENDIX C: Procedure for ICP-OES analysis

### **DAY 1- SOLUTION PREPARATION**

#### **1. Preparation of 8M Nitric Acid**

- Approximately half of 1000 mL volumetric flask is filled with deionised water.
- 550 mL of concentrated HNO<sub>3</sub> is measured and added into volumetric flask
- Balance of volumetric flask is added with deionised water to the 1000 mL mark. The volumetric flask is shaken thoroughly and allowed to cool.

#### **2. Preparation of Blank HNO<sub>3</sub> Standard**

- Measure 10 mL of concentrated HNO<sub>3</sub> and add it to 100 mL volumetric flask.
- Balance of volumetric flask is added with deionised water to the 100mL mark. The volumetric flask is shaken thoroughly and allowed to cool.

#### **3. Preparation of Phosphorus Standard**

- 0.1857 g of NH<sub>4</sub>H<sub>2</sub>PO<sub>4</sub> is weighted and added into in a small beaker.
- The beaker is topped up with deionised water, and heated until the entire sample is dissolved
- Approximately half of 1000 mL volumetric flask is filled with deionised water.
- The dissolve sample is added into the volumetric flask and topped it up with deionised water to the 1000 mL mark.
- The volumetric flask is shaken well to homogenize the solution
- Prepare four 100 mL volumetric flask.

- 50 mL of P standard is titrated from 1000 mL volumetric flask into the first 100 mL volumetric flask. The 100 mL volumetric flask is then filled with deionised water to the mark and shaken it well.
- 50 mL of P standard is titrated from first 100 mL volumetric flask into the second 100 mL volumetric flask. The 100 mL volumetric flask is then filled with deionised water to the mark and shaken it well.
- 50 mL of P standard is titrated from second 100 mL volumetric flask into the third 100 mL volumetric flask. The 100 mL volumetric flask is then filled with deionised water to the mark and shaken it well.
- 50 mL of P standard is titrated from third 100 mL volumetric flask into the last 100 mL volumetric flask. The 100 mL volumetric flask is then filled with deionised water to the mark and shaken it well

#### **4. Preparation of Vanadium Standard**

- 0.1857 g of  $\text{NH}_4\text{VO}_3$  is weighted and added into in a small beaker.
- The beaker is topped up with deionised water, and heated until the entire sample is dissolved
- Approximately half of 1000 mL volumetric flask is filled with deionised water.
- The dissolve sample is added into the volumetric flask and topped it up with deionised water to the 1000 mL mark.
- The volumetric flask is shaken well to homogenize the solution
- Prepare four 100 mL volumetric flask.
- 50 mL of V standard is titrated from 1000 mL volumetric flask into the first 100 mL volumetric flask. The 100 mL volumetric flask is then filled with deionised water to the mark and shaken it well.
- 50 mL of V standard is titrated from first 100 mL volumetric flask into the second 100 mL volumetric flask. The 100 mL volumetric flask is then filled with deionised water to the mark and shaken it well.
- 50 mL of V standard is titrated from second 100 mL volumetric flask into the third 100 mL volumetric flask. The 100 mL volumetric flask is then filled with deionised water to the mark and shaken it well.

- 50 mL of V standard is titrated from third 100 mL volumetric flask into the last 100 mL volumetric flask. The 100 mL volumetric flask is then filled with deionised water to the mark and shaken it well

### **5. Preparation of Cobalt Standard**

- 0.1561 g of  $\text{Co}(\text{NO}_3)_2$  is weighted and added into in a small beaker.
- The beaker is topped up with deionised water, and heated until the entire sample is dissolved
- Approximately half of 1000 mL volumetric flask is filled with deionised water.
- The dissolve sample is added into the volumetric flask and topped it up with deionised water to the 1000 mL mark.
- The volumetric flask is shaken well to homogenize the solution
- Prepare four 100 mL volumetric flask.
- 10 mL of Co standard is titrated from 1000 mL volumetric flask into the first 100 mL volumetric flask. The 100 mL volumetric flask is then filled with deionised water to the mark and shaken it well.
- 50 mL of Co standard is titrated from first 100 mL volumetric flask into the second 100 mL volumetric flask. The 100 mL volumetric flask is then filled with deionised water to the mark and shaken it well.
- 50 mL of Co standard is titrated from second 100 mL volumetric flask into the third 100 mL volumetric flask. The 100 mL volumetric flask is then filled with deionised water to the mark and shaken it well.
- 50 mL of Co standard is titrated from third 100 mL volumetric flask into the last 100 mL volumetric flask. The 100 mL volumetric flask is then filled with deionised water to the mark and shaken it well

### **6. Preparation of Cobalt Standard**

- 0.01 g of sample is weighed and dissolved it a few mL of 8M  $\text{HNO}_3$ .
- The beaker is heated and stirred to ensure complete dissolved.
- The dissolved sample is added into 100 mL volumetric flask.
- Balance of volumetric flask is added with 8M  $\text{HNO}_3$  to the 100mL mark. The volumetric flask is shaken thoroughly and allowed to cool.

## APPENDIX D: Preparation of Solutions Used in Redox Titration

**i. Preparation of 2M H<sub>2</sub>SO<sub>4</sub>**

Molarity for 95% of H<sub>2</sub>SO<sub>4</sub>

$$= \frac{\text{Density of } H_2SO_4}{\text{Molecular Weight of } H_2SO_4} \times \frac{95}{100} \times 1000$$

$$= \frac{1.84 \text{ gcm}^{-3}}{98.07 \text{ gmol}^{-1}} \times \frac{95}{100} \times 1000 = 14.53 \text{ molL}^{-1} = 17.82 \text{ M}$$

$$M_1V_1 = M_2V_2$$

where,

$$M_1 = \text{Concentration of 95\% of } H_2SO_4 \text{ (17.82 M)}$$

$$V_1 = \text{Volume of 95\% of } H_2SO_4$$

$$M_2 = \text{Concentration of 2 M } H_2SO_4$$

$$V_2 = \text{Volume of 2 M } H_2SO_4$$

$$M_1V_1 = M_2V_2$$

$$(17.82 \text{ M})V_1 = (2 \text{ M})(1000 \text{ mL})$$

$$V_1 = 112.2 \text{ mL}$$

Thus, 112.2 mL of 95 % of HNO<sub>3</sub> was diluted to 1000 mL volumetric flask with deionised water.

**ii. Preparation of 0.1M H<sub>2</sub>SO<sub>4</sub>**

$$M_1V_1 = M_2V_2$$

where,

$$M_1 = \text{Concentration of 95\% of H}_2\text{SO}_4 \text{ (17.82 M)}$$

$$V_1 = \text{Volume of 95\% of H}_2\text{SO}_4$$

$$M_2 = \text{Concentration of 0.1 M H}_2\text{SO}_4$$

$$V_2 = \text{Volume of 2 M H}_2\text{SO}_4$$

$$M_1V_1 = M_2V_2$$

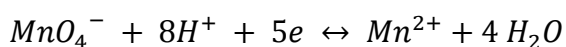
$$(17.82 \text{ M})V_1 = (0.1 \text{ M})(1000 \text{ mL})$$

$$V_1 = 5.6 \text{ mL}$$

Thus, 5.6 mL of 95 % of HNO<sub>3</sub> was diluted to 1000 mL volumetric flask with deionised water.

**iii. Preparation of 0.01 N Potassium Permanganate, KMnO<sub>4</sub>**

$$\text{Normality, } N \text{ (eq/L)} = \text{Molarity, } M \text{ (mol/L)} \times n \text{ (eq/mol)}$$



$$\text{Molarity, } M = \frac{\text{Normality, } N}{n} = \frac{0.01 \text{ N}}{5} = 0.002 \text{ molL}^{-1}$$

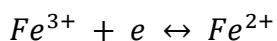
Mass of KMnO<sub>4</sub>

$$= 0.002 \text{ molL}^{-1} \times 158.04 \text{ gmol}^{-1} = 0.3161 \text{ gL}^{-1}$$

Thus, 0.3161 g of KMnO<sub>4</sub> was transferred into 1000 mL volumetric flask and top up with 0.1 M H<sub>2</sub>SO<sub>4</sub>.

**iv. Preparation of 0.01 N Ammonium Iron (II) Sulphate,  
(NH<sub>4</sub>)<sub>2</sub>Fe(SO<sub>4</sub>)<sub>2</sub>·6H<sub>2</sub>O**

Normality,  $N$  (eq/L) = Molarity,  $M$  (mol/L)  $\times$   $n$ (eq/mol)



$$Molarity, M = \frac{Normality, N}{n} = \frac{0.01 N}{1} = 0.01 \text{ molL}^{-1}$$

Mass of (NH<sub>4</sub>)<sub>2</sub>Fe(SO<sub>4</sub>)<sub>2</sub>·6H<sub>2</sub>O

$$= 0.01 \text{ molL}^{-1} \times 391.99 \text{ gmol}^{-1} = 3.92 \text{ gL}^{-1}$$

Thus, 3.92 g of (NH<sub>4</sub>)<sub>2</sub>Fe(SO<sub>4</sub>)<sub>2</sub>·6H<sub>2</sub>O was transferred into 1000 mL volumetric flask and top up with 0.1 M H<sub>2</sub>SO<sub>4</sub>.

**v. Preparation of Diphenylamine, Ph<sub>2</sub>NH<sub>2</sub> indicator**

1 g of diphenylamine was weighed and dissolved in a few ml of concentrated sulphuric acid, H<sub>2</sub>SO<sub>4</sub>. Then the solution was transferred to a 100 ml volumetric flask and further top up with concentrated H<sub>2</sub>SO<sub>4</sub>.

## APPENDIX E: Procedure for Redox Titration

### **DAY 1- SOLUTION PREPARATION**

#### **1. Preparation of Diphenylamine, Ph<sub>2</sub>NH<sub>2</sub> indicator**

- 1.00g of diphenylamine is weighed and dissolved it in few mL of concentrated H<sub>2</sub>SO<sub>4</sub>
- The solution is then transferred into 100mL volumetric flask and topped up with concentrated H<sub>2</sub>SO<sub>4</sub> till the mark of 100mL.

#### **2. Preparation of 2 M Sulphuric Acid**

- Approximately half of 1000 mL volumetric flask is filled with deionised water.
- 113 mL of concentrated H<sub>2</sub>SO<sub>4</sub> is measured and added into volumetric flask.
- Balance of volumetric flask is added with deionised water to the 1000 mL mark. The volumetric flask is shaken thoroughly and allowed to cool.

#### **3. Preparation of 0.1 M Sulphuric Acid**

- Approximately half of 1000 mL volumetric flask is filled with deionised water.
- 5.6 mL of concentrated H<sub>2</sub>SO<sub>4</sub> is measured and added into volumetric flask.
- Balance of volumetric flask is added with deionised water to the 1000 mL mark. The volumetric flask is shaken thoroughly and allowed to cool.

#### 4. Preparation of 0.01 N Ammonium Iron (II) Sulphate,



- 3.92 g of  $(\text{NH}_4)_2\text{Fe}(\text{SO}_4)_2 \cdot 6\text{H}_2\text{O}$  is weighed and dissolved in a few mL of concentrated  $\text{H}_2\text{SO}_4$
- Approximately half of 1000 mL volumetric flask is filled with 0.1 M  $\text{H}_2\text{SO}_4$ .
- The dissolved  $(\text{NH}_4)_2\text{Fe}(\text{SO}_4)_2 \cdot 6\text{H}_2\text{O}$  is then transferred into 1000 mL volumetric flask and topped up with 0.1 M  $\text{H}_2\text{SO}_4$  till the mark of 1000 mL. The volumetric flask is shaken thoroughly and allowed to cool.

### DAY 2- SOLUTION PREPARATION

#### 1. Preparation of 0.01 N Potassium Permanganate, $\text{KMnO}_4$

- 0.3161 g of  $\text{KMnO}_4$  is weighed and dissolved in a few mL of concentrated  $\text{H}_2\text{SO}_4$
- Approximately half of 1000 mL volumetric flask is filled with 0.1 M  $\text{H}_2\text{SO}_4$ .
- The dissolved  $\text{KMnO}_4$  is then transferred into 1000 mL volumetric flask and topped up with 0.1 M  $\text{H}_2\text{SO}_4$  till the mark of 1000 mL. The volumetric flask is shaken thoroughly and allowed to cool.

### DAY 2- SAMPLE PREPARATION

#### 1. Preparation of Sample Solution

- 0.10 g of sample is weighed and dissolved in a few mL of concentrated  $\text{H}_2\text{SO}_4$
- Approximately half of 100 mL volumetric flask is filled with 2 M  $\text{H}_2\text{SO}_4$ .
- The dissolved sample is then transferred into 100 mL volumetric flask and topped up with 2 M  $\text{H}_2\text{SO}_4$  till the mark of 100 mL. The volumetric flask is shaken thoroughly and allowed to cool.

## RUNNING REDOX TITRATION

### 1. Preparation of Apparatus

- 2 burette are set up using retort stand.
- 1 is filled with  $\text{KMnO}_4$  solution while the other is filled with  $(\text{NH}_4)_2\text{Fe}(\text{SO}_4)_2 \cdot 6\text{H}_2\text{O}$  solution
- Both the burettes are filled more than the  $0 \text{ cm}^3$  mark and some solution are allowed to flow through the burette till it reached the  $0 \text{ cm}^3$  mark.

### 2. Preparation of Sample for Analysis

- Each sample from the 100 mL volumetric flask is transferred into 5 conical flask (each  $20 \text{ cm}^3$ )

### 3. Running the Analysis

- 3 conical flasks are titrated with  $\text{KMnO}_4$  solution (recorded as  $V_1$ ). The colour changes observed is from original solution colour to pale purple/pink colour.
- 2 drops of  $\text{Ph}_2\text{NH}_2$  indicator are added into each conical flask and the mixture is shaken. The colour changes observed is from purple/pink colour solution to dark purple.
- It is then titrated with  $(\text{NH}_4)_2\text{Fe}(\text{SO}_4)_2 \cdot 6\text{H}_2\text{O}$  solution (recorded as  $V_2$ ). Titration is stopped when the dark purple colour changes back to the original solution colour.
- The additional 2 conical flask are added with 2 drops of  $\text{Ph}_2\text{NH}_2$  indicator and is shaken. The colour changes observed is from original solution colour to dark purple.
- It is then titrated with  $(\text{NH}_4)_2\text{Fe}(\text{SO}_4)_2 \cdot 6\text{H}_2\text{O}$  solution (recorded as  $V_3$ ). Titration is stopped when the dark purple colour changes back to the original solution colour.

## APPENDIX F: Crystallite Size Measurements by Using Powder XRD Technique

Crystallite Size,  $T$  given by Debye-Scherrer equation

$$T = \frac{0.89\lambda}{\beta_{hkl} \cos\theta_{hkl}}$$

where

$T$  = crystallite size

$\lambda$  = wavelength

$\beta$  = full-width at half maximum at  $hkl$  phase

$\theta$  = diffraction angle at  $hkl$  phase

$$\beta_{hkl} = FWHM(rad) = FWHM(^{\circ}) \times \frac{\pi}{180^{\circ}}$$

### Sample Calculation for VPOCo-24

Given  $\lambda_{CuK\alpha} = 1.54 \text{ \AA}$

3 strongest peaks from XRD

Peak No	$2\theta$ ( $^{\circ}$ )	$\theta$ ( $^{\circ}$ )	FWHM ( $^{\circ}$ )	FWHM (rad)
5	22.8755	11.4378	0.32070	0.0056
8	28.3943	14.1972	0.23950	0.0042
9	29.8943	14.9472	0.24470	0.0043

Peak appears at at  $2\theta = 22.8755$  corresponds to [0 2 0] phase

$$T = \frac{0.89\lambda}{\beta_{hkl} \cos \theta_{hkl}} = \frac{0.89(1.54)}{0.0056 \cos(11.4378)} = 249.7 \text{ \AA}$$

Peak appears at at  $2\theta = 28.3943$  corresponds to [2 0 4] phase

$$T = \frac{0.89\lambda}{\beta_{hkl} \cos \theta_{hkl}} = \frac{0.89(1.54)}{0.0042 \cos(14.1972)} = 338.2 \text{ \AA}$$

#### Sample Calculation for VPOCo-48

Peak No	$2\theta$ (°)	$\theta$ (°)	FWHM (°)	FWHM (rad)
5	22.8903	11.4452	0.38830	0.0068
8	28.4201	14.2101	0.28100	0.0049
9	29.9242	14.9621	0.28830	0.0050

Peak appears at at  $2\theta = 22.8903$  corresponds to [020] phase

$$T = \frac{0.89\lambda}{\beta_{hkl} \cos \theta_{hkl}} = \frac{0.89(1.54)}{0.0068 \cos(11.4452)} = 206.3 \text{ \AA}$$

Peak appears at at  $2\theta = 28.4201$  corresponds to [204] phase

$$T = \frac{0.89\lambda}{\beta_{hkl} \cos \theta_{hkl}} = \frac{0.89(1.54)}{0.0049 \cos(14.2101)} = 288.3 \text{ \AA}$$

## APPENDIX G: Calculation of P/V and Co/V mole ratio by using ICP-OES analysis

$$\frac{P}{V} = \frac{\text{Concentration of P/Atomic Weight of P}}{\text{Concentration of V/Atomic Weight of V}}$$

$$\frac{Co}{V} = \frac{\text{Concentration of Co/Atomic Weight of Co}}{\text{Concentration of V/Atomic Weight of V}}$$

Sample Calculation for VPOCo-24

$$\frac{P}{V} = \frac{(4.7830 \text{ mg/L})/(30.9738 \text{ mg/L})}{(8.9040 \text{ mg/L})/(50.9415 \text{ mg/L})} = 0.8835$$

$$\frac{Co}{V} = \frac{(0.124 \text{ mg/L})/(58.9332 \text{ mg/L})}{(8.9040 \text{ mg/L})/(50.9415 \text{ mg/L})} = 0.012$$

Sample Calculation for VPOCo-48

$$\frac{P}{V} = \frac{(1.990 \text{ mg/L})/(30.9738 \text{ mg/L})}{(3.924 \text{ mg/L})/(50.9415 \text{ mg/L})} = 0.8341$$

$$\frac{Co}{V} = \frac{(0.063 \text{ mg/L})/(58.9332 \text{ mg/L})}{(3.924 \text{ mg/L})/(50.9415 \text{ mg/L})} = 0.0139$$

APPENDIX H: Calculation for Average Oxidation State of Vanadium ( $V_{AV}$ )

According to Niwa and Murakami,

$$V^{4+} + 2V^{3+} = 20 [\text{MnO}_4^-] V_1$$

$$V^{5+} + V^{4+} + V^{3+} = 20 [\text{Fe}^{2+}] V_2$$

$$V^{5+} = 20 [\text{Fe}^{2+}] V_3$$

$$[\text{MnO}_4^-] = 0.01 \text{ N}$$

$$[\text{Fe}^{2+}] = 0.01 \text{ N}$$

$$V^{4+} + 2V^{3+} = 0.2 V_1 \quad \text{--- (1)}$$

$$V^{5+} + V^{4+} + V^{3+} = 0.2 V_2 \quad \text{--- (2)}$$

$$V^{5+} = 0.2 V_3 \quad \text{--- (3)}$$

(2) – (3)

$$V^{4+} + V^{3+} = 0.2 (V_2 - V_3) \quad \text{--- (4)}$$

$$V^{4+} = 0.2 (V_2 - V_3) - V^{3+} \quad \text{--- (5)}$$

Substitute (5) into (1)

$$0.2 (V_2 - V_3) + V^{3+} = 0.2 V_1$$

$$V^{3+} = 0.2 (V_1 - V_2 + V_3) \quad \text{--- (6)}$$

Substitute (6) into (5)

$$V^{4+} = 0.4 (V_2 - V_3) - 0.2 V_1$$

Therefore

$$V^{3+} = 0.2 (V_1 - V_2 + V_3)$$

$$V^{4+} = 0.4 (V_2 - V_3) - 0.2 V_1$$

$$V^{5+} = 0.2 V_3$$

Average oxidation number

$$V_{AV} = \frac{3V^{3+} + 4V^{4+} + 5V^{5+}}{V^{3+} + V^{4+} + V^{5+}}$$

Sample Calculation for  $\text{VOHPO}_4 \cdot 1.5\text{H}_2\text{O}$

<b><math>\text{VOHPO}_4 \cdot 1.5\text{H}_2\text{O}</math></b>	<b><math>\text{KMnO}_4</math>, <math>V_1</math></b>			<b><math>(\text{NH}_4)_2\text{Fe}(\text{SO}_4)_2 \cdot 6\text{H}_2\text{O}</math>, <math>V_2</math></b>			<b><math>(\text{NH}_4)_2\text{Fe}(\text{SO}_4)_2 \cdot 6\text{H}_2\text{O}</math>, <math>V_3</math></b>	
	<b>1</b>	<b>2</b>	<b>3</b>	<b>1</b>	<b>2</b>	<b>3</b>	<b>1</b>	<b>2</b>
Initial Volume ( $\text{cm}^3$ )	34.5	0.0	10.3	13.4	24.2	34.7	0.0	0.0
Final Volume ( $\text{cm}^3$ )	45.0	10.3	19.9	24.2	34.7	46.0	0.0	0.0
Volume Used ( $\text{cm}^3$ )	10.5	10.3	9.6	10.8	10.5	11.3	0.0	0.0
Average Used ( $\text{cm}^3$ )	10.1			10.9			0.0	

$$V^{3+} = 0.2 (10.1 - 10.9 + 0.0) = -0.16 \approx 0.00$$

$$V^{4+} = 0.4 (10.9 - 0) - 0.2 (10.1) = 2.34$$

$$V^{5+} = 0.2 (0.0) = 0.00$$

$$V_{AV} = \frac{3(0) + 4(2.34) + 5(0)}{0 + 2.34 + 0} = 4.000$$

Sample Calculation for VPOCo-24

VOHPO <sub>4</sub> ·1.5H <sub>2</sub> O	KMnO <sub>4</sub> , V <sub>1</sub>			(NH <sub>4</sub> ) <sub>2</sub> Fe(SO <sub>4</sub> ) <sub>2</sub> ·6H <sub>2</sub> O, V <sub>2</sub>			(NH <sub>4</sub> ) <sub>2</sub> Fe(SO <sub>4</sub> ) <sub>2</sub> ·6H <sub>2</sub> O, V <sub>3</sub>	
	1	2	3	1	2	3	1	2
Initial Volume (cm <sup>3</sup> )	0.0	4.7	9.3	0.0	7.8	16.0	26.5	28.4
Final Volume (cm <sup>3</sup> )	4.7	9.3	14.4	7.8	16.0	23.4	28.4	29.6
Volume Used (cm <sup>3</sup> )	4.7	4.6	5.1	7.8	8.2	7.4	1.9	1.2
Average Used (cm <sup>3</sup> )	4.8			7.8			1.6	

$$V^{3+} = 0.2 (4.8 - 7.8 + 1.6) = -0.28 \approx 0.00$$

$$V^{4+} = 0.4 (7.8 - 1.6) - 0.2 (4.8) = 1.52$$

$$V^{5+} = 0.2 (1.6) = 0.32$$

$$V_{AV} = \frac{3(0) + 4(1.52) + 5(0.32)}{0 + 1.52 + 0.32} = 4.17$$

Sample Calculation for VPOCo-48

VOHPO <sub>4</sub> ·1.5H <sub>2</sub> O	KMnO <sub>4</sub> , V <sub>1</sub>			(NH <sub>4</sub> ) <sub>2</sub> Fe(SO <sub>4</sub> ) <sub>2</sub> ·6H <sub>2</sub> O, V <sub>2</sub>			(NH <sub>4</sub> ) <sub>2</sub> Fe(SO <sub>4</sub> ) <sub>2</sub> ·6H <sub>2</sub> O, V <sub>3</sub>	
	1	2	3	1	2	3	1	2
Initial Volume (cm <sup>3</sup> )	30.7	32.0	33.2	30.4	32.9	34.8	0.0	0.0
Final Volume (cm <sup>3</sup> )	32.0	33.2	34.0	32.9	34.8	37.9	0.0	0.0
Volume Used (cm <sup>3</sup> )	1.3	1.2	0.8	2.5	1.9	3.1	0.0	0.0
Average Used (cm <sup>3</sup> )	1.1			2.5			0.0	

$$V^{3+} = 0.2 (1.1 - 2.5 + 0.0) = -0.28 \approx 0.00$$

$$V^{4+} = 0.4 (2.5 - 0) - 0.2 (1.1) = 0.78$$

$$V^{5+} = 0.2 (0.0) = 0.00$$

$$V_{AV} = \frac{3(0) + 4(0.78) + 5(0)}{0 + 0.78 + 0} = 4.000$$

APPENDIX I: Calculation for TPR in H<sub>2</sub> Analysis

*Total Oxygen Removed (atom/g)*

$$= \text{Amount of Oxygen Removed (mol/g)} \times 6.022 \times 10^{23} \text{ atom/mol}$$

Sample Calculation for VOHPO<sub>4</sub>·1.5H<sub>2</sub>O

For maxima temperature peak at 1009 K

*Total Oxygen Removed (atom/g)*

$$= 1.677 \times 10^{-3} \times 6.022 \times 10^{23} = 1.0101 \times 10^{21} \text{ atom/g}$$

Sample Calculation for VPOCo-24

For maxima temperature peak at 745 K

*Total Oxygen Removed (atom/g)*

$$= 2.093 \times 10^{-4} \times 6.022 \times 10^{23} = 1.260 \times 10^{20} \text{ atom/g}$$

For maxima temperature peak at 1047 K

*Total Oxygen Removed (atom/g)*

$$= 1.186 \times 10^{-3} \times 6.022 \times 10^{23} = 7.142 \times 10^{20} \text{ atom/g}$$

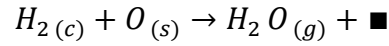
Sample Calculation for VPOCo-48

For maxima temperature peak at 1055 K

*Total Oxygen Removed (atom/g)*

$$= 1.293 \times 10^{-3} \times 6.022 \times 10^{23} = 7.787 \times 10^{20} \text{ atom/g}$$

APPENDIX J: Calculation for Reduction Activation Energy ( $E_r$ ) for TPR in  $H_2$   
Analysis



Where

- (s) = Surface or lattice oxygen species
- (c) = Chemisorbed species
- (g) = Gaseous Species
- = Oxygen Vacancy

$$Rate = k[O_s][H_2]_m$$

$$-\frac{d[H_2]}{dt} = A \exp\left(-\frac{E_r}{RT_m}\right) [O_s][H_2]_m \quad - (1)$$

Setting the derivate of equation (1) to zero at  $T_m$  gives modified version of Redhead (1962) equation:

$$\frac{E_r}{RT_m^2} = \left(\frac{A_r}{\beta}\right) [H_2]_m \exp\left(-\frac{E_r}{RT_m}\right) \quad - (2)$$

From the Arrhenius (1889) equation

$$k_1 = A \exp\left(-\frac{E_r}{RT_m}\right) \quad - (3)$$

Therefore from equation (2)

$$k_2 = A [H_2]_m \exp\left(-\frac{E_r}{RT_m}\right) \quad - (4)$$

Since  $k_1$  and  $k_2$  are the same at  $T_m$  and let  $k = \chi$  at  $T_m$

$$\frac{\chi}{A [H_2]_m} = \exp\left(-\frac{E_r}{RT_m}\right) \quad \text{or} \quad \frac{A [H_2]_m}{\chi} = \exp\left(\frac{E_r}{RT_m}\right)$$

$$\frac{E_r}{RT_m} = \ln\left(\frac{A [H_2]_m}{\chi}\right)$$

$$E_r = RT_m \ln\left(\frac{A [H_2]_m}{\chi}\right)$$

Where

$$R = 0.001987 \text{ kcal K}^{-1} \text{ mol}^{-1} ; 82.056 \text{ cm}^3 \text{ atm K}^{-1} \text{ mol}^{-1}$$

$$A = 10^{13} \text{ s}^{-1}$$

$$T_m = \text{Maxima Temperature of the Peak}$$

$$E_r = \text{Reduction Activation Energy}$$

#### Sample Calculation for VOHPO<sub>4</sub>·1.5H<sub>2</sub>O

For maxima temperature peak at 1009 K

$$\begin{aligned} E_r &= RT_m \ln\left(\frac{A [H_2]_m}{\chi}\right) \\ &= (0.001987)(1009) \ln\left(\frac{(1 \times 10^{13}) (2.045 \times 10^{-6})}{0.03754}\right) \\ &= 40.33 \text{ kcal/mol} \times \frac{4.184 \text{ J}}{1 \text{ cal}} = 168.74 \text{ kJ/mol} \end{aligned}$$

#### Sample Calculation for VPOCo-24

For maxima temperature peak at 745 K

$$\begin{aligned} E_r &= RT_m \ln\left(\frac{A [H_2]_m}{\chi}\right) \\ &= (0.001987)(745) \ln\left(\frac{(1 \times 10^{13}) (2.045 \times 10^{-6})}{0.03754}\right) \\ &= 29.78 \text{ kcal/mol} \times \frac{4.184 \text{ J}}{1 \text{ cal}} = 124.59 \text{ kJ/mol} \end{aligned}$$

For maxima temperature peak at 1047 K

$$\begin{aligned}
 E_r &= RT_m \ln \left( \frac{A [H_2]_m}{\chi} \right) \\
 &= (0.001987)(1009) \ln \left( \frac{(1 \times 10^{13}) (2.045 \times 10^{-6})}{0.03754} \right) \\
 &= 41.85 \text{ kcal/mol} \times \frac{4.184 \text{ J}}{1 \text{ cal}} = 175.09 \text{ kJ/mol}
 \end{aligned}$$

Sample Calculation for VPOCo-48

For maxima temperature peak at 1055 K

$$\begin{aligned}
 E_r &= RT_m \ln \left( \frac{A [H_2]_m}{\chi} \right) \\
 &= (0.001987)(1055) \ln \left( \frac{(1 \times 10^{13}) (2.045 \times 10^{-6})}{0.03754} \right) \\
 &= 42.17 \text{ kcal/mol} \times \frac{4.184 \text{ J}}{1 \text{ cal}} = 176.43 \text{ kJ/mol}
 \end{aligned}$$